CIAMTIS

U.S. DOT Region 3 University Transportation Center

Development of Low-Cost Weigh-In-Motion (WIM) and Response Spectra Techniques

Prepared by:

L.B. Wang, University of Georgia;
M.M. Abbas, Virginia Tech;
F. Dai, West Virginia University;
D.G. Ildefonzo, Virginia Tech;
J. Liu, Virginia Tech

r3utc.psu.edu

PennState College of Engineering

LARSON TRANSPORTATION INSTITUTE

Technical Report Documentation Page

1. Report No.	2. Government Accession No.	3. Recipient's Catalog No.
CIAM-UTC-REG13		

4. Title and Subtitle	5. Report Date
Development of Low-Cost Weigh-In-Motion (WIM) and Response Spectra Techniques; Phase I of "Development of a Cost-Effective Sensing System for Integrated Traffic and Pavement Response Monitoring in Support of Pavement Management"	September 2022
	6. Performing Organization Code

7. Author(s)	8. Performing Organization Report No.
Linbing Wang https://orcid.org/0000-0003-2670-376X, Montasir M. Abbas https://orcid.org/0000-0002-9938-0255, Fei Dai https://orcid.org/0000-0002-8868-2821, Dylan G. Ildefonzo https://orcid.org/0000-0002-3172-244X, Jian Liu	

9. Performing Organization Name and Address	10. Work Unit No. (TRAIS)
Center for Smart and Green Civil Systems The Charles E. Via, Jr. Department of Civil and Environmental Engineering Virginia Tech 750 Drillfield Drive, 200 Patton Hall Blacksburg, VA 24061	**11. Contract or Grant No.** 69A3551847103

12. Sponsoring Agency Name and Address	13. Type of Report and Period Covered
U.S. Department of Transportation Research and Innovative Technology Administration 3rd Fl, East Bldg E33-461 1200 New Jersey Ave, SE Washington, DC 20590	Final Report 3/1/2019 – 8/15/2022
	14. Sponsoring Agency Code

15. Supplementary Notes

Work funded through The Pennsylvania State University through the University Transportation Center Grant Agreement, Grant No. 69A3551847103.

16. Abstract

In recent years, an increase in heavy truck traffic has resulted in damage and service life reduction to roadway infrastructure. As a result, the demand for more weight compliance checkpoints has increased. Weight checkpoint operations have increasingly shifted to the adoption of weigh-in-motion (WIM) as a means of ensuring weight compliance. However, installing permanent WIM systems can be costly, and budget constraints can often lead to removal of weight enforcement altogether. To remedy this, a low-cost WIM system that utilizes off-the-shelf components has been developed. The system, dubbed the Roadway Infrastructure and Vehicle Information System (RIVIS), uses an array of roadside, surface-mounted accelerometers to measure pavement response to a moving load. The system has been deployed for limited testing and has shown promise for vehicle detection from pavement response. Preliminary analysis of the collected data has been completed and shows that the system has potential for use as a combined traffic monitoring and WIM system. Future work will include refinement of the system to execute identification and weighing tasks.

17. Key Words	18. Distribution Statement
Weigh-in-motion, pavement response, pavement vibration	No restrictions. This document is available from the National Technical Information Service, Springfield, VA 22161

19. Security Classif. (of this report)	20. Security Classif. (of this page)	21. No. of Pages	22. Price
Unclassified	Unclassified	49	

DISCLAIMER

Table of Contents

List of Figures

List of Tables

CHAPTER 1

Introduction

BACKGROUND

The number of annual highway ton-miles is a key metric used to track the amount of cargo transported by highways each year. From the year 2004 to the year 2014, annual highway ton-miles in the United States increased from 4.6 billion to 5.9 billion ton-miles [1], a net increase of 26%. As cargo transported by highways is overwhelmingly transported by heavy truck traffic, this figure signifies a drastic increase in heavy truck traffic on an already overburdened highway system. Overloaded trucks have caused exponential amounts of damage to transportation infrastructure, including pavements and bridges, and have drastically reduced the service life of these critical transportation assets [2]. To address the impact of overloaded trucks on transportation infrastructure, weigh-in-motion (WIM) systems have been adopted to support transportation infrastructure management and to serve as vehicle weight compliance checkpoints [3]–[8]. However, the WIM systems presently in use are costly to install and maintain, and thus are often foregone at the cost of the condition and longevity of highway infrastructure [5].

The need to develop a low-cost, portable system capable of determining vehicle weights and classification is thus necessary. This project seeks to develop such a system using a system composed of surface-mounted accelerometers located at the roadside hard shoulder. The system was designed to measure asphalt concrete pavement's response to a moving vehicle load and use the pavement response as a means of detecting vehicle presence, classifying the vehicle, and quantifying the vehicle's load.

Measurement of Pavement Response

The use of pavement response to a moving vehicle load has long been a topic of interest for transportation engineers. Mamlouk (1997) suggested that the concept of vehicle-pavement interaction could be applied to weigh-in-motion, as well as pavement design and performance management [9]. Many later studies would show this concept coming to fruition with a variety of devices and topologies. Selected relevant literature pertaining to this topic is briefly reviewed.

Arraigada, et al. (2009) showed that accelerometers were a valid means of collecting data by which pavement deflections under traffic loading could be determined [10]. Bajwa et al. (2011) exhibited the ability of pavement-embedded accelerometers to classify vehicles based on their generated pavement vibration response at the sensor location [11]. They later showed the potential of a WIM device to be developed based on the same principles [12]. Ye et al. (2020) showed the potential for a distributed MEMS accelerometer array embedded in a transverse direction in the pavement to detect vehicle location, traffic direction, and traffic volume based on pavement response [13]. This was later deployed to include a cloud computing platform for data retention and analysis [14].

Huang et al. (2018) showed the potential of a roadside system for traffic monitoring but were not fully successful in collecting the desired traffic information via this method [15]. Stocker et al. (2016) successfully deployed a machine learning algorithm for classification of vehicles based on pavement

vibrations collected from beneath the pavement [16]. Zhao et al. developed a low-cost system based on embedded piezoelectric sensors for the identification of pavement dynamic loads [17].

The selected literature reviewed shows the potential for the use of accelerometers to measure pavement responses, which can then be used to identify various parameters related to vehicle and traffic loading. One major gap noted in the literature is that presently, no system using surface-mounted accelerometers has been successfully developed and deployed. One system, that developed by Huang et al., did show some promise for this task, but failed to gather the desired information; no further work was completed to remedy the problems encountered with this system.

Accordingly, it was determined that there exists a need to further explore the use of a surface-mounted system for the measurement of pavement response acceleration with the goal of vehicle identification.

Benefits of Roadside Surface-Mounted Sensors

Surface-mounted sensors hold many benefits over traditional embedded sensors for the measurement of pavement response. Chief among these benefits is the ability to change, adjust, and maintain the sensors once they have been installed on the roadway. Owing to their position, surface-mounted sensors can be readily accessed by engineers and road crews at any point during their service life. In comparison, embedded sensors are placed within the pavement and thus are not readily accessible or adaptable to change. This is especially important when battery-operated sensors are being used. When embedded, sensors powered by batteries have an extremely limited service life; when these sensors are affixed to the surface, however, service life can be greatly extended, as the battery can be readily accessed and refreshed.

Another benefit seen with surface-mounted sensors is the ability to avoid permanently damaging the pavement on which the sensors are installed. Embedded sensors require pavement to be damaged to be installed. Often, the area of pavement damaged is the area immediately adjacent to the sensor, and material interfaces are created between the bulk of the pavement and the location of the sensor. After this point, the sensors are then generally embedded in a resin or other non-asphaltic material. To truly gain insight on the nature of pavement response, it is desirable to have measurements from a physically continuous pavement material that is free from initial defects and interfaces with large amounts of non-asphaltic materials. A further benefit is recognized in that no specialized equipment is required to install surface-mounted sensors, since no asphalt removal or replacement is needed.

Due to their quick installation time (around 2 hours total for the sensors discussed in this report), surface-mounted sensors can avoid longer-term lane closures. This can potentially reduce the impact to traffic flows, including increased delay, on the roadways and networks on which sensors are being installed.

Finally, surface mounting provides a degree of flexibility that is not present in embedded sensors. Systems incorporating surface-mounted sensors are easily accessible should additional adjustment be needed, should the network need to be expanded, or should components need replacement.

OBJECTIVES

This project has been undertaken with the objective of developing a low-cost, long-life WIM system based on the principle of pavement dynamic response. Initially, the goal of the project was to use an existing technology, namely the piezoelectric energy harvester (PEH). However, the potential of other, newer technologies with less impact on the roadway material was recognized, and efforts were instead focused on using these technologies.

Accordingly, the goal of this project was to develop a system capable of measuring pavement response for traffic and pavement monitoring. Such system was to be deployable to the field to assist in the collection of pavement and traffic data that would in turn be used in later projects to better the state of the art for pavement asset management and maintenance decision-making processes.

Moreover, the task objectives of this project were as follows:

1. Design the Pavement Response Measurement Weigh-In-Motion system ("the system")
2. Fabricate the system
3. Conduct a laboratory evaluation of the system
4. Conduct an on-site evaluation of the system
5. Perform design optimization and cost-effectiveness analysis

CHAPTER 2

Methodology

INTRODUCTION

This section of the report describes the methodology used to develop, test, and deploy the system used for the measurement of pavement response to moving vehicle loads. It is hypothesized that by measuring and analyzing the pavement dynamic response to moving load, information related to vehicle weight may be able to be gathered. The system developed for the measurement of pavement response generated by moving vehicle loads has been dubbed RIVIS, an acronym for **R**oadway **I**nfrastructure and **V**ehicle **I**nformation **S**ystem. The theory, development, testing, and deployment of RIVIS are discussed in this section.

DEVELOPING RIVIS

The Roadway Infrastructure and Vehicle Information System (RIVIS) was developed by the research team at the Center for Smart and Green Civil Systems at Virginia Tech. The goal of developing this system was to enable the measurement of pavement response using sensors that could be mounted on the pavement surface. Once developed, the system would then be deployed for data collection in attempts to further the outlined objectives of this project. The requirements for the system, the developed topology, and the equipment selected for use are discussed in the subsequent subsections of this report.

System Requirements

Several requirements were considered when developing RIVIS. The first requirement of the system was that it be as simple as possible while still being able to accomplish the task at hand. This would aid in the maintenance and troubleshooting aspects that are inherent to any system. By minimizing the number and complexity of system components, the need for maintenance is reduced and troubleshooting is more easily achieved.

Second, it was required that the system be low-cost. This requirement was interpreted in terms of both initial costs and lifecycle costs. It was found that in order to minimize both initial and lifecycle costs, the system should be designed to incorporate as many off-the-shelf, that is, commercially available components as possible. Commercially available components are beneficial because the high expense of design, development, and testing is borne by the manufacturer of the component, then amortized across each component. The end user thus benefits from a reduced cost and a well-developed and ready-to-use component. A further advantage of commercially available components is recognized in that the manufacturer often provides quality guarantees and product support over at least some of the lifecycle of the product.

Third, the system was required to be able to modularly support many different sensor types. This factor aids in facilitating any rapid changes to the system that might be necessary, as well as any rapid prototyping. While modularity was considered to be of key importance, it was also noted that in keeping with other

requirements, it was necessary to reduce the number of software packages used. Accordingly, it was determined that any data acquisition units used should be able to operate using a single software package.

Fourth, the topology of the system needed to be such that it can be installed rapidly, with minimal to no interruption to traffic flow on the roadway in which is it installed.

Fifth and finally, the system needed to have sufficient sensitivity to detect the low-level dynamic response of the pavement under vehicle loading. The system sensitivity is largely achieved by selection of the correct accelerometers, but the selection of the data acquisition unit and the mounting of the sensors also plays a factor in the overall sensitivity of the measurements taken.

With all of these factors considered, the research team was able to specify a set of components suitable for the task of measurement of dynamic pavement response under moving vehicle loading. The topology selected for RIVIS Version 1, also called RIVIS V1.0, is discussed in subsequent sections of this report.

Components of RIVIS V1.0

Components Used

For RIVIS V1.0, several pieces of equipment were selected. The primary topology of the system is discussed in the section immediately following. However, it is important to note that the primary components of RIVIS V1.0 include sensors (SEN), a data acquisition unit (DAQ), a power supply (PSP), a power source (PSO), and data storage media (DSM). Table 2.1 lists the components used for RIVIS V1.0.

Table 2.1. RIVIS V1.0 components.

Manufacturer	Model	Quantity	Description	Component Type
PCB Piezotronics	3713F1110G	1	MEMS Triaxial Accelerometer	Sensor
PCB Piezotronics	3713B112G	1	MEMS Triaxial Accelerometer	Sensor
DATAQ Instruments	DI-4718B-U	1	Data Acquisition Unit	DAQ
DATAQ Instruments	DI-8B51-02	4	Signal Conditioner	DAQ
DATAQ Instruments	DI-8B47K-05	2	Thermocouple Amplifier	DAQ
Siglent Technologies	SPD-3303X	1	Isolated DC Power Supply	PSP
Tycon Solar	RPST12-24	1	Solar Panel	PSO
Renogy	Rover	1	Solar Charge Controller	PSO
Tycon Solar	(Not Listed)	2	Solar Batteries	PSO
Western Digital	MyPassport	1	2TB Solid State Drive	DSM

Several considerations were made when selecting each piece of equipment for RIVIS V1.0. For all components, quality, cost, ease of integration, and ease of acquisition were considered before the component was specified.

Among the most important components in the RIVIS V1.0 system are the sensors chosen to measure pavement response, namely the accelerometers. For this project, micro electro-mechanical systems (MEMS) accelerometers were identified as the most viable solution due to their size, accuracy, and relatively low cost. Past research has also shown that MEMS accelerometers are a viable solution for the measurement of pavement response for pavement performance [18]–[20] and traffic and vehicle monitoring [13], [21]. An evaluation of the relevant past research also reveals several different specification

requirements for the accelerometers. The required resolution of the sensors was to be a minimum of 500 µg [11], [12], [18] with a minimum bandwidth of 50 Hz [11], [12], [18], [22] and a minimum range of ± 200 mg (the unit g refers to the standard gravitational force, 1 g = 9.81 m/s^2) [11], [12], [18]. Various sampling frequencies ranging from 64 to 1,000 Hz were suggested for optimal detection of vibrational responses [11], [12], [15], [18], [19], [22]–[24]. This information was cautiously considered as a baseline for the selection of sensors, as the fundamental nature of the systems in this literature were all based on an embedded sensor design.

Ultimately, two different MEMS sensors were selected based on the aforementioned selection criteria. The accelerometers selected were the 3713B112G and the 3713F1110G DC Response MEMS accelerometers from PCB Piezotronics. The relevant specifications for these sensors are listed in Table 2.2. Two ranges were selected for the accelerometers, ± 2 g and ± 10 g, as the sensitivity required for the problem at hand was not known at the time of purchase; this information could only be verified through testing of the sensors under the desired application. Accordingly, it was decided that two different sensitivities should be selected to mitigate risk of inadequate performance. In addition to fulfilling the selection criteria, the selected accelerometers exhibited the best specifications for their price at the time of purchase.

Table 2.2. Accelerometer specifications.

Accelerometer Model	Sensitivity	Range	Current Consumption	Excitation Voltage	Broadband Resolution
3713B112G	1,000 mV/g	±2 g	≤ 6.0 mA	6 to 30 VDC	0.35 mg rms
3713F1110G	135 mV/g	±10 g	≤ 15.0 mA	5 to 32 VDC	0.25 mg rms

After selection of the accelerometers, it was necessary to select a data acquisition unit that both exhibited high degrees of performance and flexibility and would integrate well with the selected accelerometers. Past literature recommended a minimum analog-to-digital conversion (ADC) resolution of 12 bits for DAQs handling pavement acceleration measurements [11], [12], [18], [22]. The selection criteria for the DAQ thus required a minimum resolution of 12 bits in addition to several other criteria. Included in the additional criteria was the requirement that the DAQ accept multiple inputs beyond the accelerometers. Accepting multiple inputs would allow for a single DAQ to be used for multiple sensor inputs. Another requirement was expandability to multiple channels while remaining under a single operating software; this would allow for future iterations of RIVIS to be expanded to accommodate larger distributed sensor arrays. It was additionally required that the DAQ be able to operate both standalone and when linked to a computer, be able to write to external storage media, support future configuration as an IoT-enabled device, and have a relatively low initial cost.

Considering all selection criteria, the DI-4718B-U by DATAQ Instruments was selected as the DAQ for RIVIS V1.0. The system was one of the only commercially available devices to meet all of the requirements for incorporation into the RIVIS system. Relevant specifications for the DI-4718B-U are outlined in Table 2.3. In addition to the DI-4718B-U, several signal conditioning units were purchased to allow for the specified instruments to be read. The signal conditioning units included the DATAQ Instrument DI-8B51-02, a voltage signal conditioner amplifier, and the DATAQ Instrument DI-8B47K-05, a thermocouple signal conditioner and amplifier. Specifications for the DI-8B51-02 and DI-8B47K-05 units are outlined in Table 2.4 and Table 2.5, respectively. A further advantage of the selected DAQ and signal conditioners was recognized in that each channel was truly isolated from the others, allowing for measurements to be conducted on a by-sensor basis without the risk of interference from other devices on adjacent channels.

Table 2.3. DI-4718B-U selected specifications.

Parameter	Value
Sample Throughput Rate (Max)	160 kHz
Number of Channels	8 to 128
Low-Pass Filter	Programmable by channel
Signal Conditioner	8B unit selectable by channel
Resolution	12- to 16-bit
Memory	Internal, External via USB/SD

Table 2.4. DI-8B51-02 selected specifications.

Parameter	Value
Measurement	AC, DC Voltage
Range	± 5V
Bandwidth	20 kHz

Table 2.5. DI-8B47K-05 selected specifications.

Parameter	Value
Measurement	Temperature
Range	0 ºC to 500 ºC
Thermocouple Interface	K-Type

After the data acquisition unit and signal conditioning modules were selected, it was also necessary to specify a power supply for the sensors. While it is possible to use the DI-4718B-U DAQ to provide excitation current to some sensors, the selected sensors fell outside of the range where this was possible. Accordingly, it was decided that a standalone DC power supply unit would be used for the system. The Siglent SPD-3303X was selected as the power supply used for RIVIS V1.0. This unit was selected because it contains three individually programmable channels, allowing the two accelerometers to remain isolated from one another during the measurement process. Further, the system has a relatively compact form factor, relatively low power consumption, and relatively low cost.

Upon completing the selection of all devices requiring mains power or equivalent, that is, devices that are not battery operated, the current consumption was calculated, and the solar power system was selected. Using manufacturer specifications, the maximum instantaneous consumption of the sensors, DAQ, and power supply was computed at 6.8 W. In consideration of a worst-case scenario in which the system were to run continuously for 24 hours, the daily energy demand of the system was computed as 0.163 kWh. Based on this demand, the Tycon RPST12-100-80 remote solar power system was selected. With a 12 V, 20 A continuous output, the system was sized to be able to handle the maximum instantaneous load of the system, while also providing a surplus to charge two 104 amp-hour batteries for times when the solar panel was not able to power the batteries directly.

In addition to the power and sensing components, RIVIS V1.0 also incorporated a motion-triggered camera. The camera was used to record video data, which was in turn used to validate the data collected by the other sensors during testing. The camera selected for the project was the GoPro Hero 9, which was used for both

the laboratory and closed-course trials. The Hero 9 was selected, as it provided excellent video quality, excellent motion detection, a wide-angle lens, and long battery life.

In the section that follows, a topology of the system has been provided to show the relationship between each of the selected components for RIVIS V1.0.

System Topology

Once individual components were selected, it was necessary to determine the electrical topology of RIVIS V1.0. The electrical topology of the system describes the integration of the components into a single system. Figure 2.1 shows the topology of the system as designed.

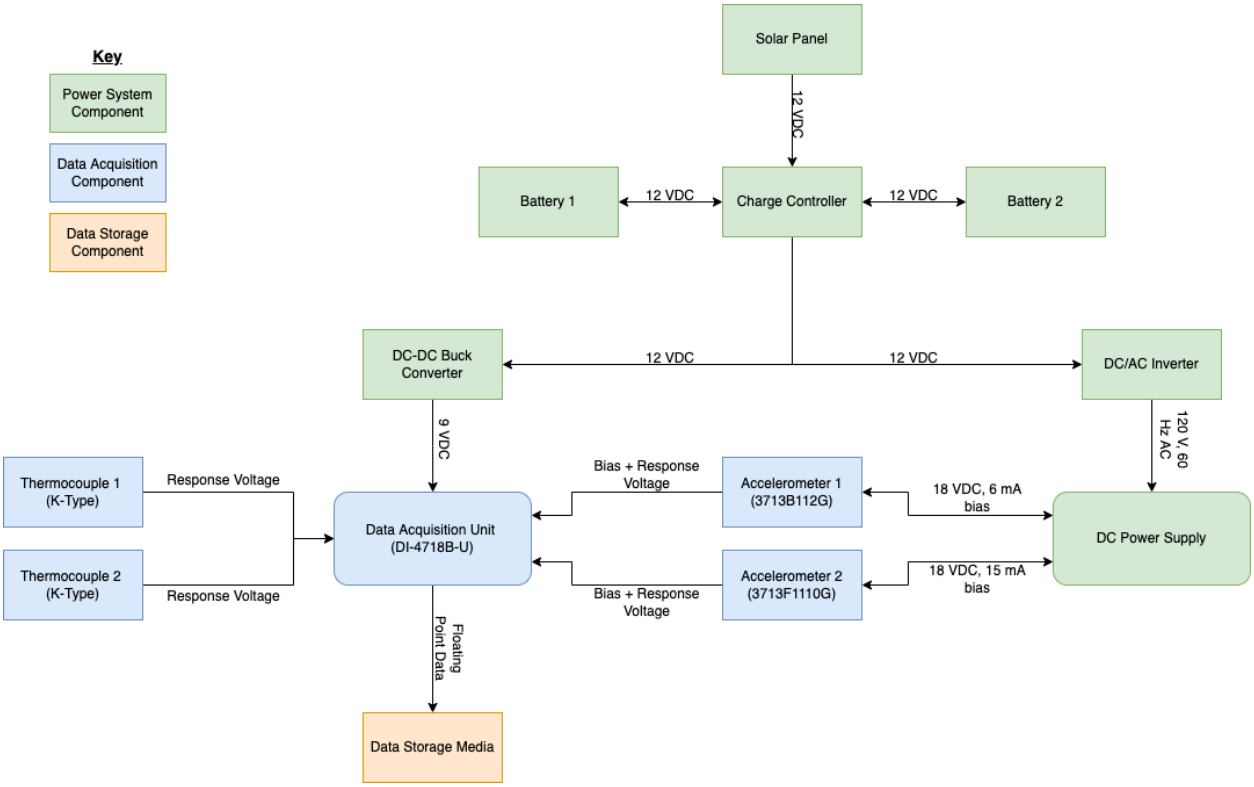

Figure 2.1. RIVIS V1.0 system topology.

TESTING RIVIS V1.0

Once developed, RIVIS V1.0 was tested in the laboratory using the Model Mobile Load Simulator 1/3 Scale (MMLS3) system. The MMLS3 is an automated pavement testing device used to simulate the successive loads of a chain of moving axles. The specific MMLS used in this project is a 1/3-scale device, allowing it to be suitable for indoor use in a smaller space. The goal of the initial testing was to make sure that RIVIS V1.0 was suitable for deployment in the field. Further, the testing allowed any necessary changes or adjustments to be made ahead of field deployment.

For the testing process, the MMLS3 was first set to a standard condition. The standard condition chosen for the testing reflects the median capabilities of the MMLS3 by adjusting machine parameters at or close to the mid-point of the machine's specified ranges. The MMLS3 settings used for the initial testing are

summarized in Table 2.6. Note that for the machine used, each bogie contains a single axle that loads the pavement.

Table 2.6. MMLS3 settings.

MMLS3 Parameter	Value Set for Testing
Loading Speed	3,600 bogies/hr = 1.5 m/s
Bogie Load	2.10 kN (± 0.05 kN)
Tire Pressure	700 kPa (± 7.0 kPa)

Once the machine settings were adjusted, several pavement specimens were placed within a specimen holder. The specimen holder was then placed on a steel isolation plate, which was then moved under the MMLS3 and bolted to the floor. The purpose of the isolation plate was to act as a damper and isolate the specimens from any vibrations that might be present within the laboratory facility while testing was taking place. Once in place, two of the five specimens were fitted with surface-mounted accelerometers at their edge.

Laboratory analysis of the system was conducted in conjunction with experiments for another UTC project entitled "Use of SmartRock Sensors to Monitor Pavement Condition for Supporting Maintenance Decision Making," which was conducted jointly by Penn State Altoona and Virginia Tech. Accordingly, information related to the topology of the laboratory testing closely mirrors that described in Shen et al. [25].

Source: Shen, et al. (2022) [25]

Figure 2.2. MMLS3 machine at Virginia Tech.

The topology used for RIVIS V1.0 testing is shown in Figure 2.3. Specimens L1, F2, F3, F4, and L5 were provided by Penn State. Specimens L1, F3, F4, and F5 contained embedded SmartRock sensors, which were tested according to the long-term testing protocol outlined in Shen et al. (2022) [25]. The specimens numbered F3 and L5 were instrumented with the RIVIS V1.0 accelerometers in the location of the blue dots in Figure 2.3. The accelerometers used were the PCB Piezotronics 3713F1110G (Specimen F3) and the PCB Piezotronics 3713B112G (Specimen L5). The accelerometers were connected to the DATAQ Instruments DI-4718B-U data acquisition unit, which was equipped with one DATAQ Instruments DI-8B51-02 Signal Amplifier and Conditioner unit per acceleration channel. The sensors were then connected

to the Siglent Technologies SPD1168X Linear DC power supply, which supplied the necessary DC excitation voltage to each sensor. The data acquisition unit was connected to a laptop computer running the requisite software. The laptop computer, data acquisition unit, and power supply were connected to mains power for the system test; however, it was separately verified that the system would operate normally using a solar power system composed of a 12 VDC solar panel, a charge controller and battery management system, deep-cycle batteries, and a basic DC-AC power inverter.

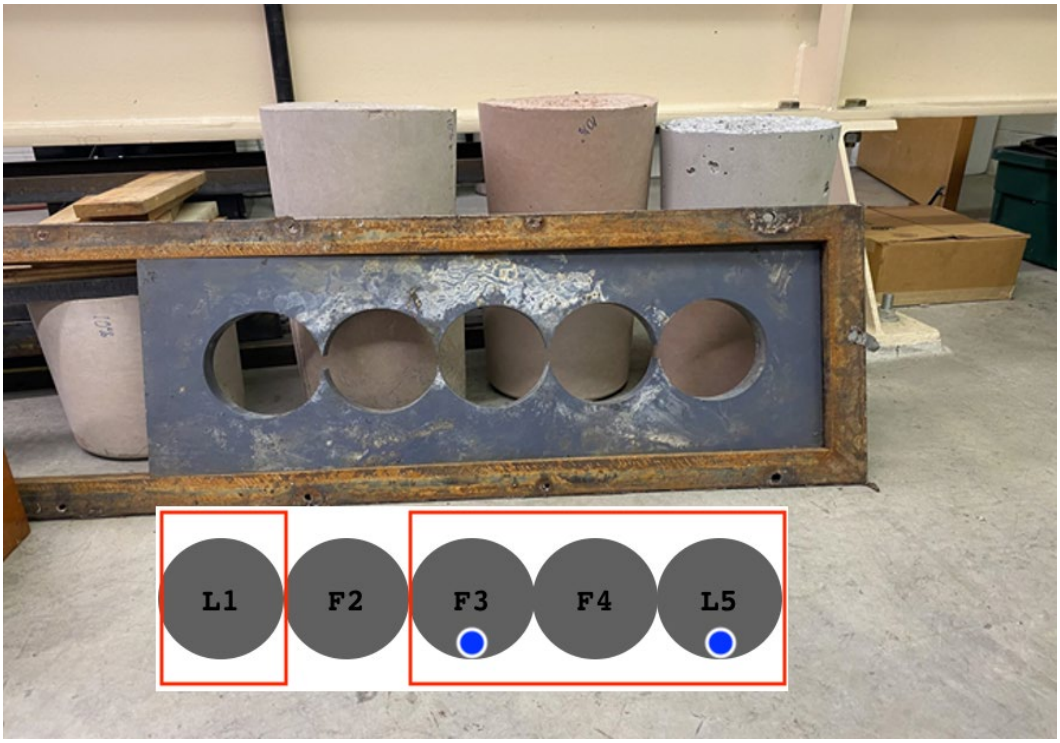

Source: Shen et al. (2022) [25]

Figure 2.3. Specimen holder (rear) and specimen topology (overlaid).

The testing of RIVIS V1.0 was conducted over a period of 40 days from September 2021 to October 2021. Over this period, the specimens to which the system was attached were subjected to 71,716 wheel loads. During the experiment described, specimens were loaded periodically, with several hour breaks taken between the loading of specimens. During the testing, the MMLS3 ran at a constant speed (axle rate) and the room in which the experiment was conducted was kept at a constant ambient temperature of 22 ºC. The results of the laboratory testing for RIVIS V1.0 are described in the "Findings" section of this report.

FIELD DEPLOYMENT OF RIVIS V1.0

A major component of the research performed under this program was the collection of pavement response data from moving vehicle loads. To limit potential corruption of the data due to outside interference, it was decided that data collection should be carried out in a closed-course, controlled environment. Accordingly, the field trials for pavement instrumented with RIVIS 1.0 were carried out on a research road at Virginia Tech in Blacksburg, Virginia. During the experiments, the roadway was closed off to outside traffic, and several vehicles completed runs up and down the closed course while the system recorded data.

Due to the limitations of the roadway and the university's research requirements, vehicles used in the experiment were property of members of the research team and were thus either passenger vehicles (FHWA

Class 2) or pickup trucks (FHWA Class 3). All vehicles used in the experiment were two-axle vehicles, and each vehicle was driven by its respective owner. A total of seven vehicles were used over two trials. Table 2.7 lists the vehicle make, model, a qualitative description of its type, and its respective U.S. Federal Highway Administration (FHWA) classification. Despite being limited to the passenger vehicle and pickup classifications, a wide array of vehicles was able to be used.

Table 2.7. Vehicle classification information.

Vehicle Make	Vehicle Model	Type Description	FHWA Class
BMW	X2	Subcompact Luxury Crossover	Class 2
Ford	F250	Heavy Duty Pickup	Class 3
Ford	Focus	Compact Hatchback	Class 2
Honda	Civic	Compact Sedan	Class 2
Mercedes-Benz	GLE-Class	Mid-Size Luxury SUV	Class 2
Mercedes-Benz	C-Class	Compact Executive Sedan	Class 2
Nissan	Titan	Pickup	Class 3
Dodge/Ram	1500	Pickup	Class 3

Prior to their participation in the experiments, information about each of the vehicles was collected. The information collected included year, make, model, tire size, tire tread depth, tire pressure, and fuel level reading. By cross-referencing open-source data published by the vehicle manufacturers, the wheelbase length, front and rear track widths, gross vehicle weights, and fuel tank capacities were collected for each of the vehicles. This information was retained and used to analyze the relationship between certain vehicle parameters and parameters of the pavement responses that those vehicles generated.

Once information was collected on each vehicle, the driver of each vehicle was instructed on how to complete the trial or "run" on the closed course. One complete run was defined as six passes of each sensor. Drivers were instructed to drive on the right-hand side of the roadway. To complete a run, drivers entered the vehicle, started the engine, and proceeded to the starting line of the course. Upon receiving a verbal signal from a member of the research team, the drivers proceeded to drive the vehicle down the course, turn around at the end, and then travel back to the original starting line. Once reaching the original starting line, the drivers were instructed to turn around and complete the course again. This entire process was repeated three times by each vehicle, for a total of six passes of each sensor per vehicle.

When driving the course, drivers were instructed to align their wheels with markings on the pavement. The markings were placed at a set distance from the sensor, normal to the side of the roadway, and were intended to provide a known distance between the sensor and the tire closest to the sensor. The first marking placed was 0.5 m from the surface-mounted accelerometers and was intended for passes numbered 1, 3, and 5; the second marking was placed 4.0 m from the surface-mounted sensors and was intended for passes numbered 2, 4, and 6.

While vehicles were completing their runs, the sensors were set to record. Data collected during this time include pavement acceleration response from the accelerometers, temperature, and video recordings of the vehicles completing the course. Table 2.8 provides details related to the data recorded during the experiments.

Table 2.8. Data parameters.

Data	Sampling Frequency	Precision	Resolution
Acceleration	1,000 Hz	Floating Point	13 bit
Temperature	1,000 Hz	Floating Point	13 bit
Video	60 frames/sec	N/A	1080P

The resolution value for acceleration and temperature is a function of the number of channels recording on the DAQ, as well as the sampling frequency. Resolution in bits is computed as follows:

$$R = \frac{log\left(\frac{160{,}000}{F*C}\right)}{\log(4)} + 12 \quad \ldots(2.1)$$

Where:

R = Resolution (bits)
F = Sampling frequency (Hz)
C = Number of channels recording

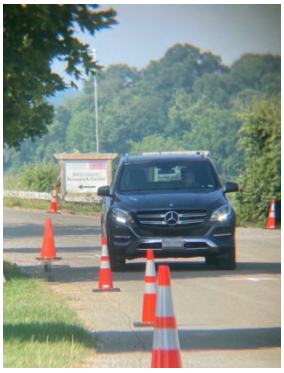

Figure 2.4. Vehicle completing a pass of the sensors.

Site Topology

The topology of the experiment site refers to the location of RIVIS V1.0 equipment within the experiment site. Figure 2.5 shows a diagram representative of the site topology.

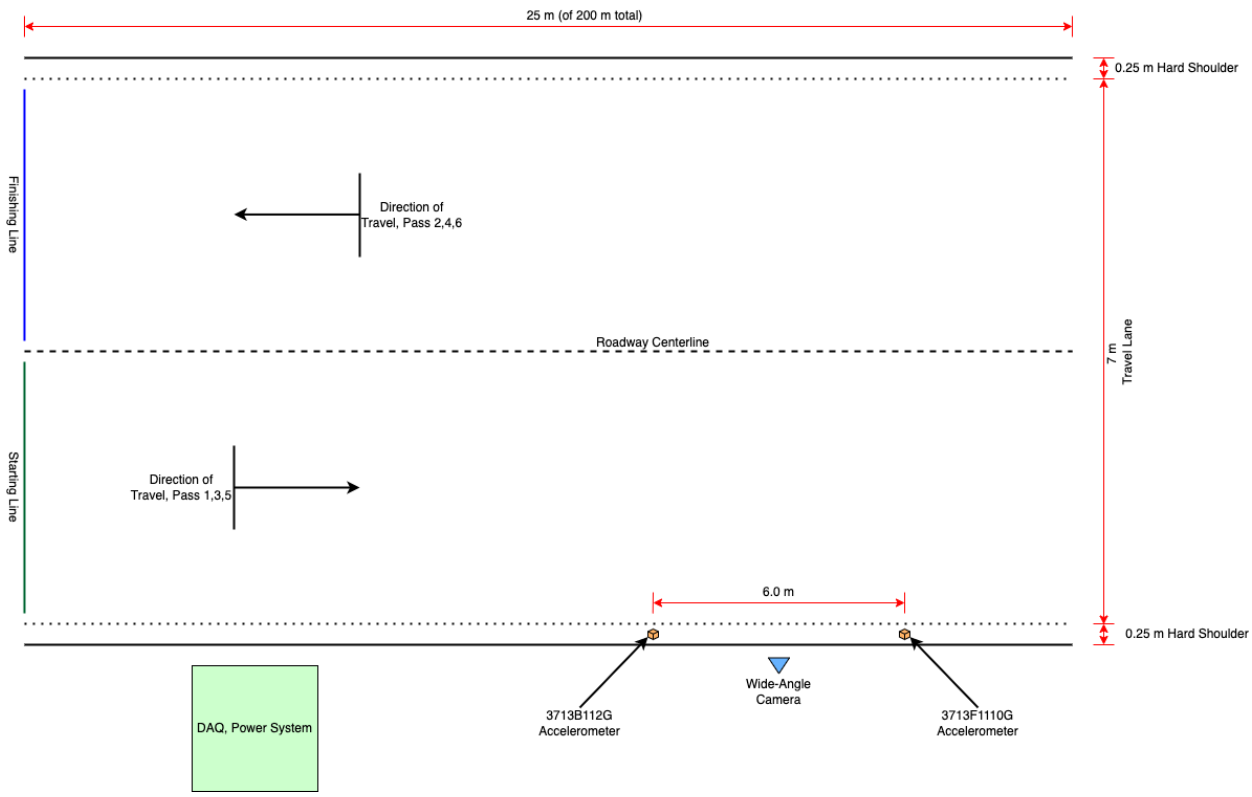

Note: Not to Scale

Figure 2.5. RIVIS V1.0 site topology.

The site topology placed the sensors, including the accelerometers and thermocouples, on the southernmost edge of the roadway. Passes 1, 3, and 5 of each vehicle's six passes were closest to the sensors, with a distance between the closest tire and the sensors of approximately 0.5 m, while passes 2, 4, and 6 were at a distance farther away from the sensors, approximately 4.0 m. When placed, the accelerometers' mounts were placed at a spacing of 6 m and affixed to the pavement using a rapid-setting two-part epoxy adhesive; the adhesive was allowed 24 hours to cure in place. After the epoxy had set, the sensors were screwed onto their mounting studs. Prior to the experiment, the data acquisition and power systems were placed on the roadside in a weatherproof enclosure, and the sensor cables were placed in cable mounts affixed to the edge of the roadway. Just before the experiments were to start, the wide-angle camera was placed at the midpoint between the sensors. The camera clock was then synchronized with the DAQ clock prior to the start of the experiments, to provide a common timestamp on all data.

The site used for experiments is located adjacent to the research team's laboratory facilities on the campus of Virginia Tech in Blacksburg, Virginia. The roadway used for the trials is known as the Inventive Lane Research Roadway, Inventive Lane, or the Research Roadway, and will be referred to by one of these names in all subsequent sections of this report. The Research Roadway is a 0.6-km-long, 7.5-m-wide roadway that provides local-level service for access to several laboratory facilities and offices. The first 0.3 km of the roadway are paved with asphalt pavement, which ultimately gives way to gravel surface for 0.3 km until the roadway's southern terminus. For the experiments completed under this project, a 0.2-km section of asphalt-paved roadway, starting about 0.1 km from the road's northern terminus point, was utilized.

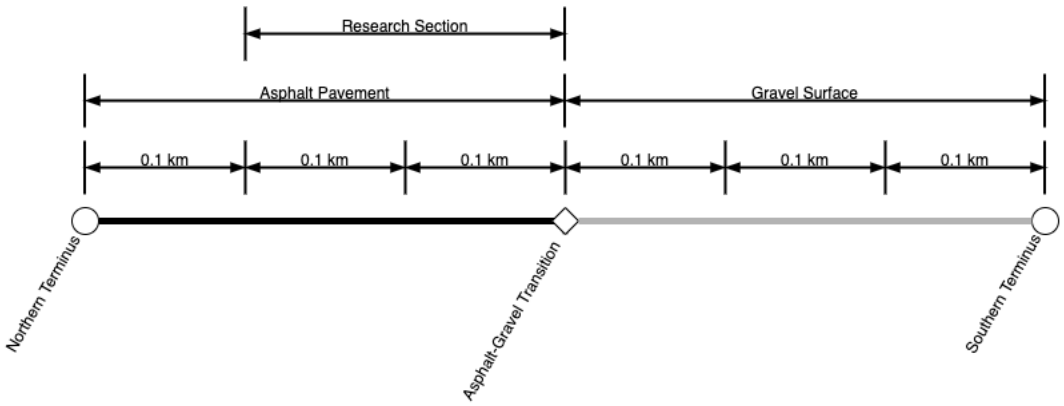

Figure 2.6. Test site pavement materials.

Figure 2.6 outlines the overall material composition of the roadway between the northern and southern terminuses; the section of the roadway used for research is notated as the Research Section. This roadway section was instrumented with several devices so that data could be collected. Devices used for data collection are discussed in the section of this report entitled "RIVIS V1.0 Components."

DATA PROCESSING

In this section, the processing of data collected during the trials is discussed. Special focus is paid to the processing of the pavement response data from the accelerometers. The data format and methodologies used for the processing of the data are discussed. Results of the data processing are discussed in Chapter 3: Findings.

Data Format

During the field trials, data were collected from the accelerometers at a sampling frequency of 1 kHz (1,000 Hz or 1,000 samples/second) for the duration of each vehicle trial. The DAQ was set to automatically output the data collected as a binary file and automatically save the output files to the storage media (in this case, an external SSD). Each data point within the binary file was written as a double-precision floating-point value. As the 64-bit depth of double-precision floating-point values far exceeds the precision of the 13-bit analog-to-digital converters present in the signal conditioners of the DAQ, the risk of premature truncation of any individual data point is eliminated.

After each vehicle run, the research team ensured that the data were successfully written to the storage media before proceeding to the next vehicle run in the trial. Each vehicle run file was labeled with the sequential order of the run within the specific trial, the name of the vehicle, and the date of the trial. Once each trial was completed, the raw data were transferred from the storage media to a desktop computer, at which point processing of the data began.

Pre-Processing the Data

In the context of this project, pre-processing of the data refers to the manipulation of the collected signals to improve the ability for the data to yield meaningful results. All pre-processing and processing of data was completed using MATLAB software.

To begin analysis of the data collected, a MATLAB script was created to convert the binary files to a usable format. The script read the binary file as an input, converted the data from binary to double-precision

floating point, labeled the data according to what it represented (for instance: time, accelerometer 1 signal, etc.), and uploaded the labeled data as arrays into the workspace.

Once in the workspace, the raw data were visualized to check for any artifacts that may impact the processing of the signal. In some instances, sharp drop-outs were seen in the signal (Figure 2.7a). To identify the nature of these drop-outs, the video footage of the trials was reviewed. From review of the time-synchronized video, it was discovered that the cause of the drop-outs was radio frequency (RF) interference between a research team member's radio and the data acquisition unit. While checking the data acquisition unit, a team member inadvertently activated their radio, causing it to broadcast RF, which corrupted the signal. It should be noted that this only occurred when the team member's radio was in direct physical contact with the DAQ; the interference could not be replicated when there was no direct physical contact between the DAQ and the radio. To remedy the interference, the sections within each signal that contained the interference were removed (as in Figure 2.7b).

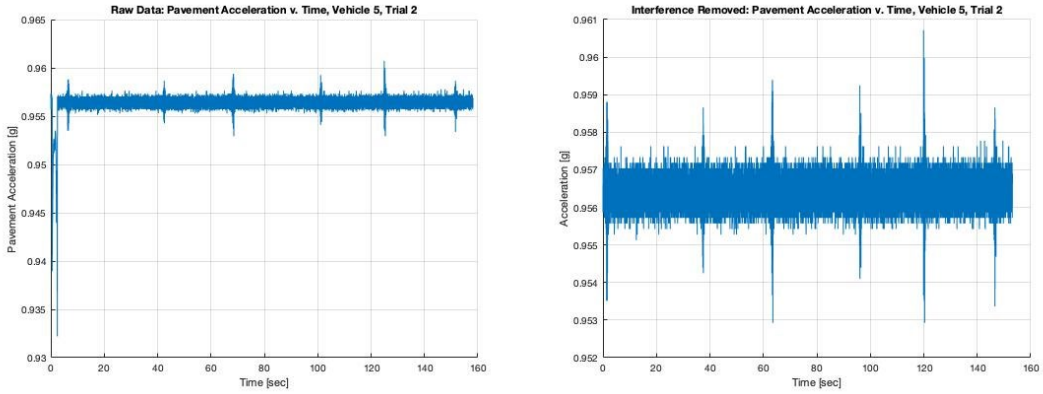

(a) (b)

Figure 2.7. (a) Signal showing RF interference at the beginning; (b) the same signal with the RF interference removed.

After instances of signal interference were removed, the acceleration signal was detrended and normalized. Detrending was carried out to remove any polynomial trends in the mean of the data, effectively creating a zero-mean signal. Normalization was carried out to provide a common baseline for comparison between all of the signals across all of the trials and vehicle runs by forcing all signals to have a median value of zero (0) and a standard deviation value of 1. Normalization resulted in the units of acceleration changing from unit g (1 g = 9.81 m/s^2) to a unitless quantity, Normalized Acceleration.

Once the signal was normalized, it was analyzed against the video footage of the trials. The timestamps on the video were compared with those on the signal, and the regions of interest were identified. Regions of interest are instances in which the vehicle passed the sensor, resulting in a pavement response that is measured by the accelerometers. After the signal ROIs were identified for each signal, the pre-processing was considered complete.

Processing the Data

Once pre-processing was completed, the data for each trial and run were processed. First, frequency domain analysis was completed. This was followed by filtering of the signals, then denoising of the filtered signals. After filtering and denoising, the ROIs were isolated from the overall signals, and descriptive statistics were

taken for each ROI. Finally, regression analysis was completed on selected ROI statistics and selected vehicle parameters.

Frequency Domain Analysis

Frequency domain analysis of all collected signals was completed using the spectrogram method. The spectrogram method uses the short-time Fourier transform (STFT) to generate a time-frequency domain representation of each input signal. To improve resolution and limit spectral leakage, a Hanning window with 50% overlap was utilized in the computation of the STFT. A MATLAB function called `findnwin()` was developed to accept the desired frequency domain resolution for the spectrogram as an input variable and output the appropriate size and number of windows for each signal. Once computed, the spectrograms for each signal were visualized and the visualizations were analyzed.

In addition to computation of the spectrogram for each signal, the power spectral density (PSD) of each signal ROI was also computed by the fast Fourier transform (FFT) method. Computation of the individual FFT for each ROI was completed using Welch's method, with a Hanning window with 50% overlap to prevent spectral leakage. Similar to the aforementioned spectrogram, the `findnwin()` function was used to determine the appropriate size and number of windows for each signal that would maintain the desired input frequency resolution. For both instances, the desired frequency resolution input was 2.0 Hz. Once computed, the frequency spectra for each ROI were visualized and analyzed against the overall spectrogram for the signals.

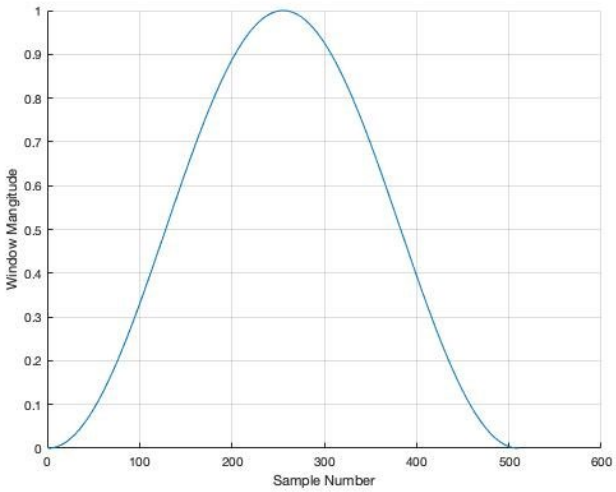

Figure 2.8. Example of a Hanning window with length of 500 samples.

From the spectrogram and the spectra of the individual ROIs, the bandwidth of each signal was estimated from the plots. In this case, the bandwidth of the signal refers to the part of the frequency spectrum over which the power of sections of signal are distributed. Identification of the bandwidth of each signal is completed to determine which frequency band contains mostly signal, and which contains mostly noise.

Analyzing the Regions of Interest

Regions of interest (ROIs) were extracted from the main signals, and the ROIs' extents were validated with time-stamped video data collected during the trials. The ROIs were then visualized and descriptive statistics were taken for each of the ROIs. Namely, the minimum and maximum values of each ROI were considered

as the most critical statistics for the purposes of this project. The maximum values of normalized acceleration in each ROI were labeled as the ROI Peak Normalized Acceleration values, and the minimum values of normalized acceleration in each ROI were labeled as the ROI Minimum Normalized Acceleration values. The ROI Peak and Minimum Normalized Acceleration values were noted for later analysis.

Completing the Regression Analysis

Regression analysis was completed to establish the relationships between vehicle parameters and certain response parameters. A total of 36 parameter-response relationships were analyzed by regression analysis.

Before completing the regression analysis, it was first necessary to prepare the data. The dataset of Peak and Minimum Acceleration values for each ROI was compiled from the detrended acceleration data. The data were divided and organized according to several different factors.

First, the dataset was divided by trial. Once divided by trial, the dataset was again split, this time into maximum ROI values and minimum ROI values. An additional subset of data was extracted to represent the ROI minimum and maximum values corresponding to the physical closeness of the vehicle to the sensor. Recall that during the field trial, each vehicle completed 6 passes, resulting in 6 signal regions of interest. ROIs 1, 3, and 5 correspond to the close passes, where the vehicle was immediately adjacent to the sensor, at a distance of approximately 0.5 m or closer. ROIs 2, 4, and 6 correspond to the far passes, where the vehicle was on the other side of the roadway and farther away from the sensors.

Once the dataset was divided, 36 different linear regression analyses were completed. Table 2.9 details the independent variable, dependent variable, and sequential number of each regression analysis completed.

Table 2.9. Details of regression analyses.

Number	Trial	Dependent Variable (Y)	Independent Variable (X)
1	1	Maximum ROI Acceleration	Vehicle Weight
2	1	Maximum ROI Acceleration	Vehicle Tire Width
3	1	Maximum ROI Acceleration	Vehicle Wheelbase
4	1	Maximum ROI Acceleration, Close Passes	Vehicle Weight
5	1	Maximum ROI Acceleration, Close Passes	Vehicle Tire Width
6	1	Maximum ROI Acceleration, Close Passes	Vehicle Wheelbase
7	1	Maximum ROI Acceleration, Far Passes	Vehicle Weight
8	1	Maximum ROI Acceleration, Far Passes	Vehicle Tire Width
9	1	Maximum ROI Acceleration, Far Passes	Vehicle Wheelbase
10	1	Minimum ROI Acceleration	Vehicle Weight
11	1	Minimum ROI Acceleration	Vehicle Tire Width
12	1	Minimum ROI Acceleration	Vehicle Wheelbase
13	1	Minimum ROI Acceleration, Close Passes	Vehicle Weight
14	1	Minimum ROI Acceleration, Close Passes	Vehicle Tire Width
15	1	Minimum ROI Acceleration, Close Passes	Vehicle Wheelbase
16	1	Minimum ROI Acceleration, Far Passes	Vehicle Weight
17	1	Minimum ROI Acceleration, Far Passes	Vehicle Tire Width
18	1	Minimum ROI Acceleration, Far Passes	Vehicle Wheelbase
19	2	Maximum ROI Acceleration	Vehicle Weight
20	2	Maximum ROI Acceleration	Vehicle Tire Width
21	2	Maximum ROI Acceleration	Vehicle Wheelbase
22	2	Maximum ROI Acceleration, Close Passes	Vehicle Weight
23	2	Maximum ROI Acceleration, Close Passes	Vehicle Tire Width
24	2	Maximum ROI Acceleration, Close Passes	Vehicle Wheelbase
25	2	Maximum ROI Acceleration, Far Passes	Vehicle Weight
26	2	Maximum ROI Acceleration, Far Passes	Vehicle Tire Width
27	2	Maximum ROI Acceleration, Far Passes	Vehicle Wheelbase
28	2	Minimum ROI Acceleration	Vehicle Weight
29	2	Minimum ROI Acceleration	Vehicle Tire Width
30	2	Minimum ROI Acceleration	Vehicle Wheelbase
31	2	Minimum ROI Acceleration, Close Passes	Vehicle Weight
32	2	Minimum ROI Acceleration, Close Passes	Vehicle Tire Width
33	2	Minimum ROI Acceleration, Close Passes	Vehicle Wheelbase
34	2	Minimum ROI Acceleration, Far Passes	Vehicle Weight
35	2	Minimum ROI Acceleration, Far Passes	Vehicle Tire Width
36	2	Minimum ROI Acceleration, Far Passes	Vehicle Wheelbase

Note that for any vehicles with a staggered tire setup—that is, with tires of different widths on the front and the rear—the average width of the front and rear tire was used as a dependent variable. This occurs in one notable case within the trial dataset, that of the Mercedes-Benz C300 (vehicle 6), where the front tires had a width of 225 mm and the rear tires had a width of 245 mm. For the regression, the tire width for this vehicle was set at 235 mm, the average of the two tire widths.

Regression was completed using MATLAB software. The nature of the dataset dictates that it is most appropriate to use binomial regression to compute the curve fit. This is because for each vehicle, each independent variable has only one constant value (for instance, there is only one tire width per vehicle), but

the resulting dependent values have multiple values; the data thus fall into a binomial distribution. Binomial regression analysis was carried out on all variable pairs listed in Table 2.10.

From the binomial regression analysis, the outputs include coefficient of determination (R^2), the coefficients p_1 and p_2, confidence bounds for p_1 and p_2, the sum of squares errors (SSE), and the root mean square error (RMSE). Using coefficients p_1 and p_2, the equation of the fit line can be determined by substitution:

$$f(x) = p_1 * x + p_2 \quad \ldots(2.2)$$

Where:

p_1, p_2 are the fit coefficients
$f(x)$ is the dependent variable at x
x is the independent variable

Results of the regression analysis are discussed in Chapter 3 of this report.

CONCLUSION

The theory, components, topology, laboratory testing, and field deployment of RIVIS V1.0, as well as the processing of collected data, have been discussed in this chapter. Data and results of both the laboratory testing and the field deployment of the system are discussed in the following chapter of this report, entitled "Chapter 3: Findings."

CHAPTER 3

Findings and Conclusions

INTRODUCTION

This section of the report discusses the findings and conclusions from various stages of the research project at hand. Findings and conclusions related to the laboratory test and the field deployment are both discussed. Justification of the validity of the proposed methodology, findings related to the nature of the data collected, and findings related to the regression analysis of the data are discussed.

A NOTE ON THE IMPACT OF THE COVID-19 PANDEMIC TO THIS PROJECT

During the design and data collection phases of this project, COVID-19 rapidly evolved from a geographically-isolated disease impacting only a small subset of individuals into a global pandemic. In the early days of the pandemic, little was known about the nature of the disease, and far less was known about adequate personal protection. Beginning in March 2020, Virginia Tech and the research team's home department enacted a moratorium on non-critical experimental research that lasted for nearly 9 months, resulting in numerous delays to the development and data collection for this project.

FINDINGS OF THE LABORATORY TEST

Findings from the laboratory deployment of RIVIS V1.0 are discussed in this section. Findings of the laboratory experiment relate to both the validity of the use of surface-mounted sensors and findings related to the components of RIVIS V1.0.

Validity of Surface-Mounted Sensors

Mounting accelerometers to the surface of pavement specimens has been shown to be a valid method of obtaining pavement vibrational response signature to moving loads in the laboratory environment. During the MMLS3 test, data were taken from two surface-mounted sensors. Visualization of the data revealed a sharp rise in the acceleration signal coinciding with the instance in time in which the wheels of the MMLS3 contacted the pavement. Time-stamped synchronized video footage of the testing was used to validate wheel presence and pavement response.

Validity of RIVIS V1.0 Components

Through laboratory testing, it was shown that the sensors, data acquisition unit, power supply, data storage media, and video capture equipment specified were all valid for the collection of pavement response to a moving load in the laboratory setting. Solar power components were also separately tested and found to provide adequate power for operation of the system in the field. The laboratory testing also revealed that the use of a rapid-setting epoxy adhesive was a valid means of mounting the sensors to the pavement surface.

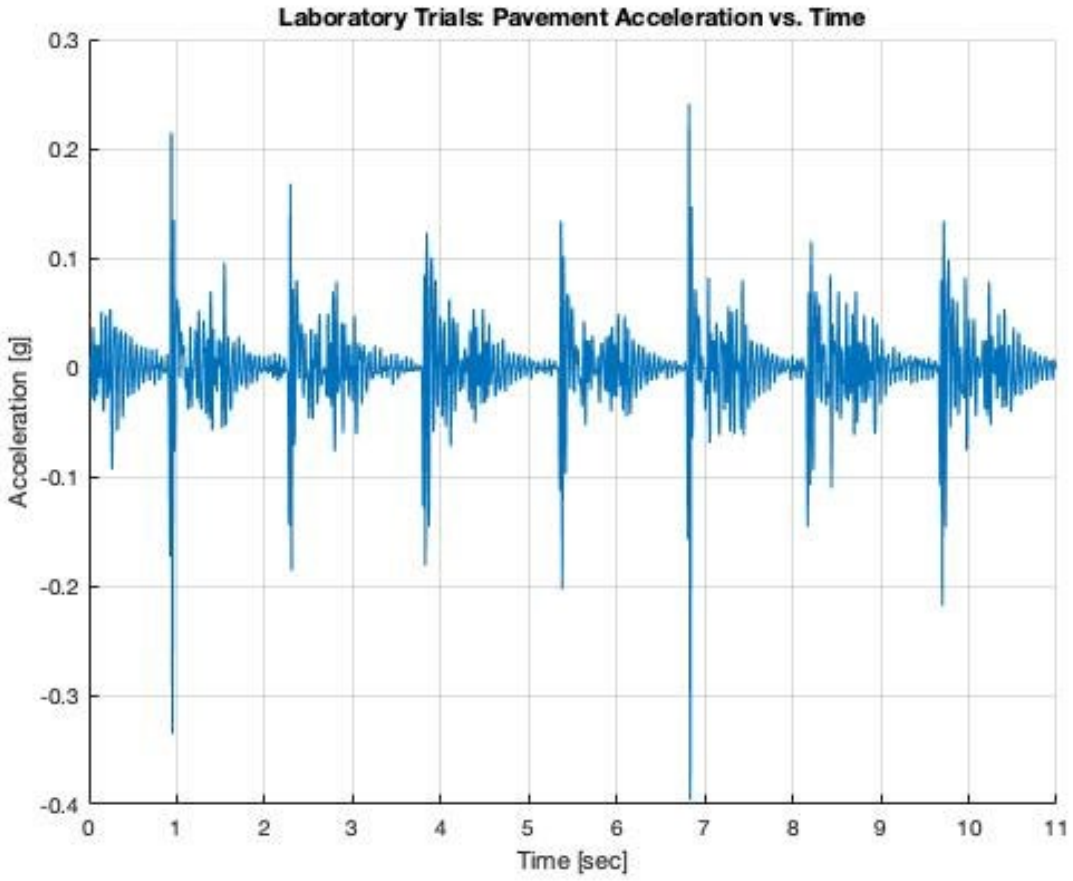

Figure 3.1. Acceleration measurement from laboratory trials.

Figure 3.1 shows the acceleration measurements from the laboratory experiment. Using time-synchronized video footage taken during the laboratory experiments, it was determined that the large peak values coincide with instances of the wheel passing the sensor.

FINDINGS OF THE FIELD DEPLOYMENT

Validity of Surface-Mounted Sensors

Visualization of both the time and frequency domain reveal that the surface-mounted accelerometers were able to record instances of moving vehicle loads passing the sensors. Accordingly, deployment of the RIVIS V1.0 system as designed was deemed as a valid means to measure pavement vibrational response.

Additionally, the use of a rapid-setting epoxy adhesive was determined to be a valid means of mounting sensors to the pavement surface in the field.

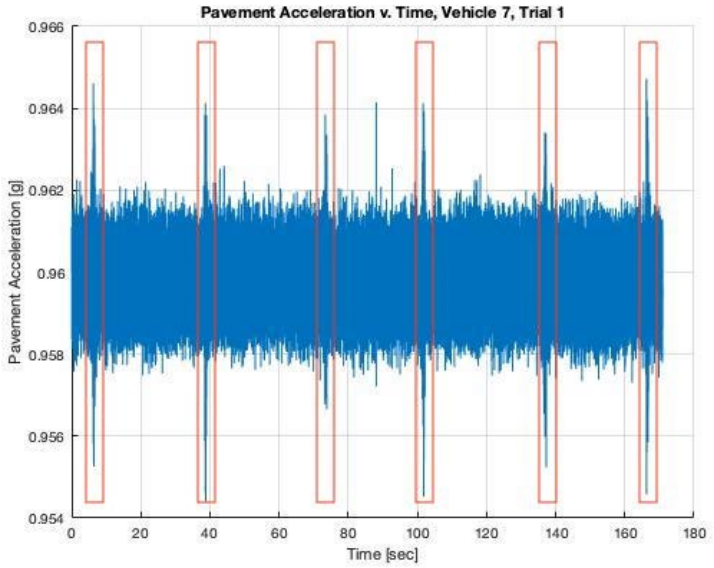

Figure 3.2. Acceleration measurement from field trials.

Figure 3.2 shows an example of the raw time-domain pavement response signal collected during the field trials. In the figure, instances of validated pavement response to moving load are outlined with orange boxes. It can be seen that as a vehicle passes the sensors, an acceleration response is generated. This response is measured by the accelerometers. Accordingly, it is shown that the selected topology for RIVIS V1.0 is in fact able to measure pavement response resulting from a moving load.

Nature of the Collected Pavement Response Signals

The nature of the raw signal data collected from the accelerometers was examined. It was found that of the 13 signals collected, nearly all the raw data had one or more issues requiring attention in pre-processing. The most common issue requiring attention was the detrending of the signals. Due to the nature of the instrumentation, a constant acceleration of 1 g (9.81 m/s^2) was present in the raw data. This was the result of the Earth's gravitational force acting in the direction of acceleration measurement. While the most common issue, this issue was easily corrected by a single line of code, which removed the measurement bias due to gravity in each case. This pre-processing can be easily automated and can be carried out between collection of the data and writing the data to the storage media.

A second issue with the signals was found in 6 of the 13 signals collected and manifested as sudden sharp drops in the signal waveform. Upon review of the footage of the trials, the cause of the signal drop-outs was determined to be radio frequency interference due to direct contact between the DAQ and a handheld radio belonging to one of the team members. It is believed that sufficient isolation of the DAQ from direct contact with any RF-producing device should remedy this problem. However, there is presently no means by which RF interference can be corrected, due to the random nature of its effects on the signal waveforms.

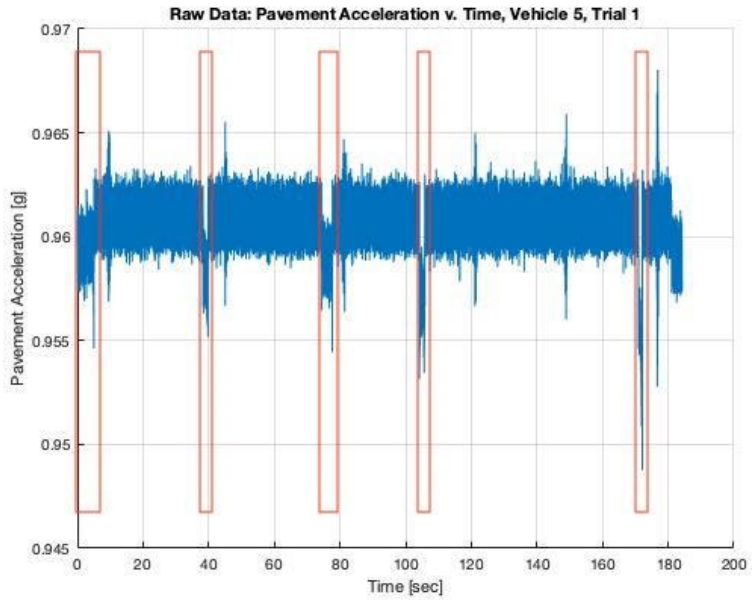

Figure 3.3. Acceleration measurement from field trials showing RF interference (outlined).

Finally, it was noted that some signals contained quantization error. Quantization error is present in the measurements due to limitations of resolution in the chosen instrumentation, namely the DAQ. Quantization error can be removed by increasing the resolution of the instrumentation. It is thus concluded that the resolution of 13 bits is insufficient due to the very small magnitude of the signals being measured.

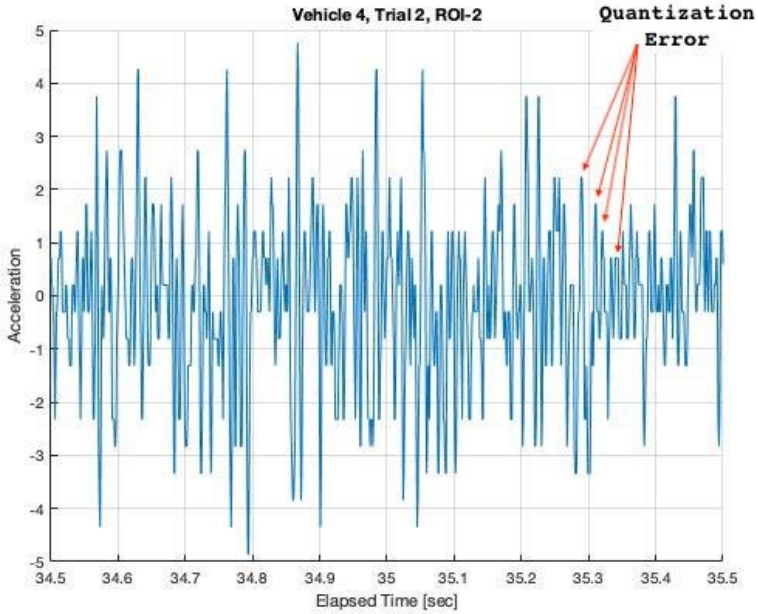

Figure 3.4. Example of quantization error in field measurements.

Figure 3.4 shows an example of quantization error. Note that the magnitudes tend to fall within certain quanta, which are limited by the resolution of the DAQ's analog-to-digital converter. If the DAQ's ADC is

unable to resolve the value of a measurement, it simply rounds the value and reports it at the next value closest to its resolution.

Frequency Domain Analysis

The analysis of the frequency domain components revealed several interesting results. First, it is noted that the time-frequency power spectrum vis the spectrogram method is a valid means of determining vehicle presence within a signal. By completing the STFT, and visualizing STFT information in the time-frequency domain, regions of relatively higher signal power occur at times that concur with the signal ROI. An example of this phenomenon can be observed in Figure 3.5.

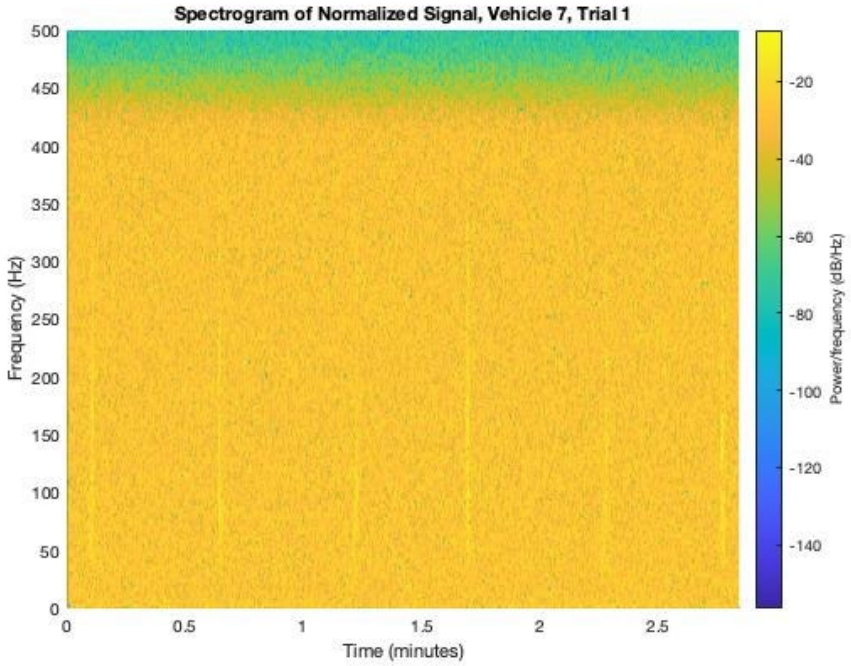

Figure 3.5. Example of spectrogram.

In Figure 3.5, regions of lighter yellow that appear as vertical bars have been found to be coincident with vehicle regions of interest. In addition, the spectrogram of the signal shows the bandwidth of the regions of interest of the signal. The bandwidth of each ROI is defined as the range of frequencies over which power is greater than the surrounding frequency bands. The bandwidth of each ROI is directly related to the bandwidth of pavement response frequencies generated by the vehicles. Accordingly, analyzing the spectrogram to find the bandwidth may prove to be a useful tool for vehicle identification. Table 3.1 lists the approximate passband frequency, stopband frequency, and bandwidth by trial of each vehicle based on its spectrogram. Spectrograms for each vehicle are included in Appendix A of this report.

Table 3.1. Signal bandwidth information.

Vehicle	Trial	Passband Frequency (Hz)	Stopband Frequency (Hz)	Estimated Bandwidth
1	2	30	200	170 Hz
2	2	45	325	280 Hz
3	1	40	225	185 Hz
	2	40	250	210 Hz
4	1	35	200	165 Hz
	2	35	200	165 Hz
5	1	45	275	230 Hz
	2	50	275	225 Hz
6	1	40	300	260 Hz
	2	45	300	255 Hz
7	1	45	300	255 Hz
	2	40	300	260 Hz
8	1	50	275	225 Hz

Analysis of the bandwidths estimated from the vehicle spectrograms indicates that for vehicles that participated in multiple trials, the bandwidth is the same or similar across trials. One exception to this is seen in vehicle 3, where the estimated bandwidth across trials differs by 25 Hz. It is important to note that the analysis of vehicle bandwidths based on their spectrograms is preliminary in nature and should be expanded upon in future research.

In addition to spectrograms, the PSD of each ROI was completed, and the predominant frequencies were noted. Table 3.2 outlines the predominant frequencies for each ROI.

Table 3.2. Predominant frequencies by ROI.

Veh.	Trial	ROI	Predominant Frequencies	ROI	Predominant Frequencies
1	2	1	60, 73, 99, 108, 152 Hz	4	5, 44, 71, 92, 138, 191 Hz
		2	7, 62, 76, 85, 99, 112, 133 Hz	5	58, 73, 106, 122, 134, 161 Hz
		3	51, 65, 81, 97, 108, 141 Hz	6	2, 30, 57, 78, 92, 118, 129, 145, 182, 212 Hz
2	2	1	55, 67, 107, 142, 182 Hz	4	60, 75, 98, 117, 160 Hz
		2	15, 62, 85, 110, 182 Hz	5	47, 60, 85, 117, 165, 205 Hz
		3	58, 87, 115, 122, 140,155, 192 Hz	6	65, 80, 107, 122, 142 Hz
3	1	1	2, 10, 24, 38, 54, 68, 93, 103, 128, 150, 194, 246, 297, 367 Hz	4	2, 8, 30, 52, 72, 90, 100, 128, 148, 202, 313 Hz
		2	4, 38, 48, 66, 92, 102, 194, 224, 263, 360 Hz	5	16, 52, 76, 104, 220, 234, 256, 277 Hz
		3	2, 8, 18, 40, 50, 76, 88, 102, 114, 136, 202, 252, 265, 260, 391 Hz	6	2, 50, 62, 78, 94, 106, 128, 176, 234, 248, 333 Hz
	2	1	20, 60, 98, 135 Hz	4	13, 55, 106, 186, 204 Hz
		2	53, 75, 100, 118 Hz	5	18, 49, 69, 124, 142, 202 Hz
		3	11, 22, 53, 98,144 Hz	6	20, 55, 84, 93, 113 Hz
4	1	1	3, 17, 45, 62, 85, 95, 115, 160, 190, 214, 254, 272, 374, 392 Hz	4	3, 20, 47, 82, 112, 125, 145, 175, 200, 234, 284, 322, 356, 409 Hz
		2	3, 15, 45, 60, 77, 97, 110, 130, 190, 217, 260, 269, 279, 372, 408 Hz	5	3, 27, 52, 72, 82, 97, 125, 142, 192, 232, 262, 312, 354, 384 Hz
		3	3, 22, 47, 77, 95, 137, 150, 222, 232, 289, 324, 342, 356 Hz	6	3, 13, 35, 47, 60, 80, 92, 102, 125, 132, 167, 212, 252, 272, 294, 329, 399 Hz
	2	1	10, 24, 36, 70, 78, 112, 142, 188 Hz	4	8, 54, 70, 118, 154 Hz
		2	2, 18, 46, 58, 76, 112, 166 Hz	5	2, 26, 42, 56, 92, 104, 120, 170, 220 Hz
		3	4, 16,36,68,120,138, 188, 212 Hz	6	18, 46, 86, 114, 130, 152 Hz
5	1	1	11, 27, 49, 78, 89, 106, 146, 175, 206, 220, 233, 257, 315 Hz	4	9, 18, 33, 51, 71, 85, 91, 100, 133, 166, 206, 237, 250, 330, 355, 404 Hz
		2	2, 22, 53, 75, 86, 102, 133, 164, 186, 239, 257, 272, 288, 337, 392 Hz	5	11, 20, 42, 57, 71, 98, 126, 211, 242, 266, 368, 408 Hz
		3	18, 33, 44, 75, 84, 98, 109, 131, 155, 177, 195, 211, 255, 271, 288, 317, 357 Hz	6	2, 24, 42, 60, 75, 93, 118, 135, 166, 208, 231, 242, 271, 299, 379 Hz
	2	1	24, 36, 54, 78, 100, 160, 196 Hz	4	52, 100, 124, 150, 202 Hz
		2	12, 56, 78, 108, 154, 176 Hz	5	72, 102, 120, 140 Hz
		3	12, 66, 80,106, 124, 140, 176, 192 Hz	6	25, 54, 85, 104, 132, 170 Hz
6	1	1	3, 40, 70, 92, 120, 157, 182, 277, 327 Hz	4	3, 22, 62, 107, 117, 127, 155, 200, 224, 264, 279, 307, 324, 369 Hz
		2	10, 37, 52, 92, 107, 157, 219, 234, 254, 277, 304, 332, 412 Hz	5	5, 13, 35, 55, 67, 82, 110, 160, 214, 232, 280, 307, 357, 392 Hz
		3	3, 45, 54, 77, 92, 112, 127, 150, 190, 229, 302 Hz	6	3, 25, 50, 65, 80, 100, 110, 125, 167, 185, 210, 230, 282, 322, 364 Hz
	2	1	16, 38, 54, 68, 84, 96, 108, 168 202 Hz	4	16, 46,66,100, 110, 130, 162, 189 Hz
		2	8, 22, 54, 94, 110, 130, 162, 190 Hz	5	28, 60, 90, 116, 132, 154, 174, 202, 222 Hz
		3	8, 50, 70, 92, 106, 132, 188 Hz	6	16, 32, 64, 94, 104, 120, 138, 190, 204 Hz
7	1	1	14, 31, 71, 91, 100, 111, 123, 145, 174, 197, 214, 234, 276, 293, 342, 376 Hz	4	11, 57, 68, 88, 100, 145, 160, 176, 210, 262, 282, 319, 387 Hz
		2	40, 60, 66, 80, 97, 123, 148, 199, 239, 274, 305, 356 Hz	5	20, 34, 57, 97, 117, 140, 157, 171, 202, 219, 242, 305, 348 Hz
		3	3, 31, 63, 68, 80, 97, 114, 143, 168, 234, 268, 288, 296, 316, 359, 399 Hz	6	17, 57, 71, 80, 94, 145, 165, 259, 328, 348 Hz
	2	1	22, 50, 72, 88, 106, 124, 144, 164 Hz	4	16, 34, 44, 76, 116, 142, 176 Hz
		2	14, 32, 52, 66, 92, 114, 136, 188 Hz	5	2, 14, 26, 62, 86, 116, 162, 174, 192, 222 Hz
		3	10, 20, 52, 68, 84, 110, 134, 156, 216, 228 Hz	6	2, 10, 62, 76, 84, 106, 120, 148 Hz
8	1	1	2, 30, 40, 52, 62, 82, 90, 102, 110, 136, 176, 216, 228, 240, 248, 277, 311, 357, 395 Hz	4	2, 16, 42, 66, 92, 104, 114, 132, 1444, 160, 180, 204, 210, 220, 236, 263, 305, 331, 399, 411 Hz
		2	2, 28, 50, 56, 68, 80, 88, 96, 118, 146, 168, 188, 208, 242, 266, 275, 315, 325, 341 Hz	5	2, 22, 52, 78, 96, 102, 120, 144, 162, 204, 240, 268, 323 Hz
		3	8, 38, 48, 94, 102, 118, 140, 178, 232, 253, 268, 293, 335, 357 Hz	6	6, 16, 40, 65, 78, 92, 110, 122, 154, 178, 212, 226, 238, 252, 301, 395 Hz

Regression Analysis

Binomial regression analysis was completed to compare vehicle parameters to the peak pavement response measured by the accelerometers during the field trials. A total of 36 individual regression analyses were completed; the independent and dependent variables for each regression analysis completed are listed in Table 2.9 in Chapter 2 of this report.

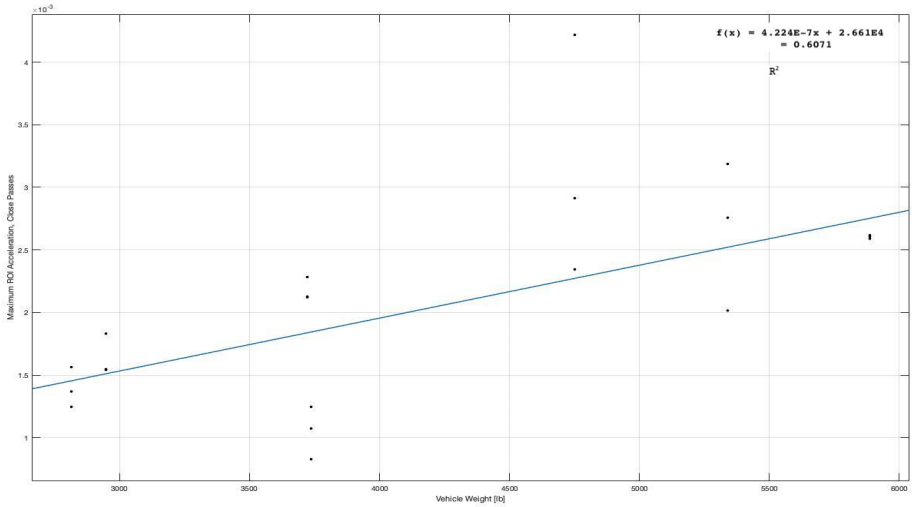

Figure 3.6. Linear regression analysis of peak ROI magnitude vs. vehicle tire width.

As previously reported, binomial regression was chosen, as the dataset was distributed in a binomial distribution. Regression analysis was completed to compare the peak and minimum ROI values for each signal to vehicle weight (unit: pounds), vehicle tire width (unit: millimeters), and vehicle wheelbase length (unit: millimeters). These vehicle parameters were either measured prior to the field trial or referenced from open-source manufacturer data. Table 3.3 presents the results of the regression analysis and includes the dependent variable name, the independent variable name, the linear fit equation, and the coefficient of determination (R^2) value.

Table 3.3. Results of regression analyses.

Number	R^2	P_1	P_2	SSE	RMSE
1	0.5443	$3.398*10^{-7}$	$2.524*10^{-3}$	$1.722*10^{-5}$	$7.177*10^{-4}$
2	0.5642	$1.058*10^{-5}$	$1.341*10^{-3}$	$1.647*10^{-5}$	$6.960*10^{-4}$
3	0.4601	$6.428*10^{-7}$	$2.010*10^{-3}$	$2.040*10^{-5}$	$7.746*10^{-4}$
4	0.3684	$4.392*10^{-7}$	$2.067*10^{-3}$	$6.138*10^{-6}$	$6.194*10^{-4}$
5	0.4021	$1.331*10^{-5}$	$6.313*10^{-4}$	$5.810*10^{-6}$	$6.026*10^{-4}$
6	0.1618	$9.516*10^{-7}$	$1.038*10^{-3}$	$8.145*10^{-6}$	$7.135*10^{-4}$
7	0.4737	$2.122*10^{-7}$	$3.134*10^{-3}$	$1.386*10^{-5}$	$9.308*10^{-4}$
8	0.4890	$7.008*10^{-6}$	$2.291*10^{-3}$	$1.346*10^{-5}$	$9.171*10^{-4}$
9	0.4145	$1.897*10^{-7}$	$3.487*10^{-3}$	$1.542*10^{-5}$	$9.817*10^{-4}$
10	0.3812	$-3.418*10^{-7}$	$-2.483*10^{-3}$	$3.644*10^{-5}$	$1.035*10^{-3}$
11	0.3780	$-1.040*10^{-5}$	$-1.345*10^{-3}$	$3.663*10^{-5}$	$1.038*10^{-3}$
12	0.2182	$-5.333*10^{-7}$	$-2.376*10^{-3}$	$4.604*10^{-5}$	$2.264*10^{-3}$
13	0.2348	$-5.077*10^{-7}$	$-1.533*10^{-3}$	$8.371*10^{-6}$	$7.233*10^{-4}$
14	0.0785	$-1.422*10^{-5}$	$-1.587*10^{-4}$	$1.020*10^{-5}$	$7.985*10^{-4}$
15	0.0473	$-9.170*10^{-7}$	$-8.956*10^{-4}$	$1.055*10^{-5}$	$8.119*10^{-4}$
16	-0.0966	$-9.063*10^{-8}$	$-4.149*10^{-3}$	$4.363*10^{-5}$	$1.651*10^{-3}$
17	-0.0923	$-4.073*10^{-6}$	$-3.517*10^{-3}$	$4.346*10^{-5}$	$1.648*10^{-3}$
18	-0.1135	$1.692*10^{-7}$	$-5.046*10^{-3}$	$4.430*10^{-5}$	$1.664*10^{-3}$
19	0.4182	$3.705*10^{-7}$	$4.677*10^{-4}$	$1.856*10^{-5}$	$6.812*10^{-4}$
20	0.3086	$1.028*10^{-5}$	$-4.188*10^{-4}$	$2.212*10^{-5}$	$7.436*10^{-4}$
21	0.3451	$6.821*10^{-7}$	$-7.708*10^{-5}$	$2.090*10^{-5}$	$7.228*10^{-4}$
22	0.6071	$4.224*10^{-7}$	$2.661*10^{-4}$	$5.202*10^{-6}$	$5.232*10^{-4}$
23	0.4729	$1.651*10^{-5}$	$-1.827*10^{-3}$	$6.979*10^{-6}$	$6.061*10^{-4}$
24	0.3733	$6.241*10^{-7}$	$6.822*10^{-5}$	$8.297*10^{-6}$	$6.608*10^{-4}$
25	0.1771	$2.984*10^{-7}$	$8.275*10^{-5}$	$1.528*10^{-5}$	$8.966*10^{-4}$
26	0.0654	$3.105*10^{-6}$	$1.360*10^{-3}$	$1.735*10^{-5}$	$9.555*10^{-4}$
27	0.2610	$7.166*10^{-7}$	$-8.579*10^{-5}$	$1.372*10^{-5}$	$8.497*10^{-4}$
28	0.2303	$-4.833*10^{-7}$	$-2.644*10^{-4}$	$3.693*10^{-5}$	$9.608*10^{-4}$
29	0.1721	$-1.119*10^{-5}$	$4.312*10^{-4}$	$3.972*10^{-5}$	$9.965*10^{-4}$
30	0.1616	$-9.522*10^{-7}$	$6.225*10^{-4}$	$4.022*10^{-5}$	$1.003*10^{-3}$
31	0.3071	$-5.638*10^{-7}$	$4.585*10^{-5}$	$1.341*10^{-5}$	$8.401*10^{-4}$
32	0.2077	$-2.006*10^{-5}$	$2.432*10^{-3}$	$1.533*10^{-5}$	$8.983*10^{-4}$
33	0.0362	$-7.036*10^{-7}$	$1.153*10^{-4}$	$1.865*10^{-5}$	$9.908*10^{-4}$
34	0.4310	$-9.095*10^{-8}$	$-1.664*10^{-3}$	$1.628*10^{-5}$	$9.258*10^{-3}$
35	0.3984	$-2.393*10^{-6}$	$-1.467*10^{-3}$	$1.772*10^{-5}$	$9.519*10^{-3}$
36	0.2597	$-1.183*10^{-6}$	$1.337*10^{-3}$	$2.119*10^{-5}$	$1.056*10^{-3}$

Each trial is analyzed individually. First, Trial 1, which is composed of numbers 1 through 18 in Table 3.2, is analyzed. From the regression analysis, the general goodness of fit, indicated by the coefficient of determination, R^2, is mostly poor. R^2 ranges from -0.1135 to 0.5642. The binomial regression models with the highest goodness of fit are number 2 (R^2 = 0.5642) and number 1 (R^2 = 0.5443). These regressions model the correlation between maximum ROI acceleration and vehicle tire width, and maximum ROI acceleration and vehicle weight, respectively. This indicates that tire width and vehicle weight are the two most closely correlated factors to the value of maximum ROI acceleration. However, due to the relatively poor fit, no further evaluation of the relationship can be determined.

Due to the poor fit in 16, 17, and 18, it can be said with relative certainty that there is no correlation between vehicle weight, vehicle tire width, and vehicle wheelbase length and the minimum ROI acceleration on those passes occurring farther from the sensor for Trial 1. Conversely, however, the maximum ROI

acceleration on those passes occurring farther from the sensor shows somewhat better correlation with values of vehicle weight, vehicle tire width, and vehicle wheelbase length, as shown by the R^2 values for numbers 7, 8, and 9.

Trial 2 is composed of numbers 19 through 36 in Table 3.2. Similar to Trial 1, the general goodness of fit is generally quite poor, with R^2 ranging from 0.0362 to 0.6071. The binomial regression models with the highest goodness of fit are number 22 ($R^2 = 0.6071$) and number 23 ($R^2 = 0.4729$). These regressions model the relationships between maximum ROI acceleration on those passes closest to the sensor and vehicle weight, and maximum ROI acceleration on those passes closest to the sensor and vehicle tire width, respectively.

Comparing the results of Trial 2 to those of Trial 1, it is noted that the strongest correlations occur between either vehicle tire width or vehicle weight and the maximum ROI acceleration values (be they for the overall signal or for the close passes). Accordingly, due to the presence of these independent variable in the best fitting models of both trials, it can be concluded that the vehicle tire width and the vehicle weight may be critical factors in the resulting pavement acceleration response measured by surface-mounted sensors.

Estimated System Cost

A major objective of RIVIS V1.0 was to develop a system with lower costs that traditional weigh-in-motion systems. Table 3.4 presents the estimated cost breakdown of RIVIS V1.0.

Table 3.4. Estimated cost breakdown.

Item	Estimated Cost*
Accelerometers	$3,750.00
Cables	$640.00
Thermocouples	$38.00
Power System	$1,600.00
Data Acquisition Unit	$700.00
Signal Conditioners	$546.00
Installation**	$1,000.00
Estimated Total Cost:	$8,974.00

*Note: all costs in U.S. Dollars.
**Note: installation estimate based on 2 hours of labor and a mobile shoulder closure.

The total cost of the RIVIS V1.0 System as installed is estimated at US$7,974.00. As the present system has two acceleration sensing nodes for measurement of pavement response, this figure breaks down to an estimated per-node cost of around $4,487.00. Hallenbeck et al. (2004) and Kwon (2016), as cited by Zhao et al. (2019), proposed similar systems for measuring pavement response with reported per-node costs of US$15,000 and US$15,250, respectively [17], [26], [27]. RIVIS V1.0 shows an approximate 73% reduction in total per-node cost compared to these systems.

It should be noted that the system proposed by Zhao et al. still slightly undercuts this pricing with a per-node cost of $3,602.50 [17]. However, monetary costs are not the only costs that bear considering when discussing systems of this type. Due to the unique location of RIVIS V1.0 on the roadway hard shoulder, only a shoulder closure is required for installation, instead of a full lane closure. This not only reduces costs associated with closing the lane, but also reduces the overall impact on traffic, improving traffic flow and reducing the costs incurred by traffic delay. Further, the cost of installing the system is predicted to be lower than that of other systems. This is because no specialized equipment is required for the installation of the system, and no changes to the pavement or surrounding infrastructure are required. During the roadway

trials, the total time taken for one person to install the entire system was around 1 hour. This short installation time reduces both monetary and opportunity costs, as a smaller crew is required for installation.

While the per-node cost of $4,487.00 does present a good overall value, system costs may be further reduced by scaling the system to include more sensing nodes. Often, discounts are applied as the number of sensors purchased increases, which then reduces the per-node cost. As the accelerometers compose the largest proportion of the system cost, it may also be possible to reduce per-node costs by selecting different accelerometers. As sensing technologies continue to evolve, the cost of advanced sensors like those used in RIVIS V1.0 continue to fall. Soon, it may be possible to obtain sensors with the same or greater performance capabilities for the same or less cost.

CHAPTER 4

Recommendations

RECOMMENDATIONS AND FUTURE WORK

Recommendations related to the findings of this report are detailed in this section. Further, the future work that should or will be undertaken in response to these recommendations is detailed.

Refinement of RIVIS V1.0 and Signal Processing Algorithms

RIVIS should be refined to improve performance, especially in terms of signal resolution. Refinement of the system to support higher resolution will allow for more information to be extracted from the collected signals. While the 13-bit resolution of the DAQ chosen for RIVIS V1.0 is sufficient to extract some useful information from the signals collected, higher-resolution measurements would provide a means for more meaningful analysis of the system.

The signal processing algorithms should be updated to account for the nature of the signals collected. Signal distortion related to drift should be removed by means of a pre-processing stage between the DAQ and storage media. Signal mean bias resulting from gravitational force should be removed from the measurements automatically in the pre-processing stage as well. Additional efforts should be dedicated to study the automatic removal of RF interference from collected signals.

Additionally, efforts should be undertaken to reduce the estimated per-node cost of the system. This may be achieved through refining the selected components to reduce costs. Due to the rapid development of new sensing technologies, it is understood that accelerometers with the same or better performance than those used in RIVIS V1.0 may soon be available at lower costs. As such, the main area identified for the reduction of costs is the replacement of the accelerometers with other components.

Additional Data Collection

Additional data collection should be carried out to validate the findings of this report. It should be noted that the data analyzed in this report represents only a limited dataset collected under controlled conditions. To establish more robust relationships between vehicle parameters such as weight and size classification and pavement response, a more varied dataset should be collected.

Presently, plans are in place to collect pavement response data on an active roadway using an updated version of RIVIS. Once these data are collected, they will be similarly analyzed for the detection of vehicle classification, speed, weight, and axle count.

Incorporation of Simulative Computational Modeling

Vehicle classification, speed, weight, and axle count should be detected from data collected using RIVIS V1.0 or a similar system that employs surface-mounted sensors and simulated response generated from

numerical modeling approaches. Simulation of vehicle loading and the associated responses using a finite element model (FEM), boundary element model (BEM), or combination FEM-BEM numerical model should be carried out. The resulting simulated responses should be used to detect vehicle presence, classification, or other parameters. Further, pavement response data collected using RIVIS V1.0 should be used to continuously update the numerical model so that it is able to more accurately predict pavement responses under a wider set of conditions.

Additionally, a more robust means of determining relationships between vehicle parameters and resulting pavement responses should be identified.

Quantifying Vehicle Loads Based on Pavement Response Spectra

In future studies, vehicle loads will be quantified based on the pavement response spectra. Using simulation of loading, the transfer function of the pavement system will be identified and analyzed. Once the transfer function is known, vehicle loads can be more easily quantified.

References

[1] M. J. Sprung and M. Chambers, *Two Decades of Change in Transportation: Reflections from Transportation Statistics Annual Reports, 1994-2014*, Washington, D.C.: U.S. Department of Transportation, Bureau of Transportation Statistics, doi: https://doi.org/10.21949/1501645.

[2] H. Wanshui, W. Jun, C. S. Cai, and C. Suren, "Characteristics and Dynamic Impact of Overloaded Extra Heavy Trucks on Typical Highway Bridges," *Journal of Bridge Engineering*, vol. 20, no. 2, p. 05014011, Feb. 2015, doi: 10.1061/(ASCE)BE.1943-5592.0000666.

[3] J. Honefanger, J. Strawhorn, R. Athey, J. Carson, G. Conner, D. Jones, T. Kearney, J. Nicholas, P. Thurber, and R. Woolley, "Commercial Motor Vehicle Size and Weight Enforcement in Europe," Washington, D.C.: U.S. Department of Transportation, Report No. FHWA-PL-07-002, 2007.

[4] B. D. Taylor, A. Bergan, N. Lindgren, and C. Berthelot, "Heavyweight Safety: Overweight Commercial Vehicles Are a Safety Hazard to Other Motorists and Have an Inordinate Impact on Infrastructure," In *Traffic Technology International: The International Review of Advanced Traffic Management*, 2000, 234-237.

[5] H. Xiong and Y. Zhang, "Feasibility Study for Using Piezoelectric-based Weigh-In-Motion (WIM) System on Public Roadway," *Applied Sciences*, vol. 9, no. 15, 2019, doi: 10.3390/app9153098.

[6] D. Cebon, *Handbook of Vehicle-Road Interaction*. Lisse, Netherlands: Swets & Zeitlinger, 1999.

[7] B. Sivakumar and F. I. Sheikh Ibrahim, "Enhancement of bridge live loads using weigh-in-motion data," *Bridge Structures*, vol. 3, no. 3–4, pp. 193–204, Sep. 2007, doi: 10.1080/15732480701515386.

[8] M. Ghosn, B. Sivakumar, and F. Moses, *Protocols for Collecting and Using Traffic Data in Bridge Design*. Washington, D.C.: National Academies Press, 2011. doi: 10.17226/14521.

[9] M. Mamlouk, "General Outlook of Pavement and Vehicle Dynamics," *J Transp Eng*, vol. 123, no. 6, pp. 515–517, Nov. 1997, doi: 10.1061/(ASCE)0733-947X(1997)123:6(515).

[10] M. Arraigada, M. N. Partl, S. M. Angelone, and F. Martinez, "Evaluation of accelerometers to determine pavement deflections under traffic loads," *Mater Struct*, vol. 42, no. 6, pp. 779–790, 2009, doi: 10.1617/s11527-008-9423-5.

[11] R. Bajwa, R. Rajagopal, P. Varaiya, and R. Kavaler, "In-Pavement Wireless Sensor Network for Vehicle Classification," In *Proceedings of the 10th International Conference on Information Processing in Sensor Networks, IPSN 2011, April 12-14, 2011, Chicago, IL, USA*, 2011.

[12] R. Bajwa, E. Coleri, R. Rajagopal, P. Varaiya, and C. Flores, "Development of a Cost Effective Wireless Vibration Weigh-In-Motion System to Estimate Axle Weights of Trucks," *Computer-Aided Civil and Infrastructure Engineering*, vol. 32, no. 6, pp. 443–457, 2017, Accessed: Feb. 20, 2019. [Online]. Available: http://research.engr.oregonstate.edu/coleri/sites/research.engr.oregonstate.edu.coleri/files/w-wim_for_truck_weights_cacaie_.pdf

[13] Z. Ye, H. Xiong, and L. Wang, "Collecting comprehensive traffic information using pavement vibration monitoring data," *Computer-Aided Civil and Infrastructure Engineering*, vol. 35, no. 2, pp. 134–149, Feb. 2020, doi: https://doi.org/10.1111/mice.12448.

[14] Z. Ye, G. Yan, Y. Wei, B. Zhou, N. Li, S. Shen, and L. Wang (2021). "Real-Time and Efficient Traffic Information Acquisition via Pavement Vibration IoT Monitoring System," *Sensors*, vol. 21, no. 8, 2021, doi: 10.3390/s21082679.

[15] Y. Huang, L. Wang, Y. Hou, W. Zhang, and Y. Zhang, "A prototype IOT based wireless sensor network for traffic information monitoring," *International Journal of Pavement Research and Technology*, vol. 11, no. 2, pp. 146–152, Mar. 2017, doi: 10.1016/j.ijprt.2017.07.005.
[16] M. Stocker, P. Silvonen, M. Rönkkö, and M. Kolehmainen, "Detection and Classification of Vehicles by Measurement of Road-Pavement Vibration and by Means of Supervised Machine Learning," *J Intell Transp Syst*, vol. 20, no. 2, 2016.
[17] Q. Zhao, L. Wang, K. Zhao, and H. Yang, "Development of a Novel Piezoelectric Sensing System for Pavement Dynamic Load Identification," *Sensors*, vol. 19, no. 21, 2019, doi: 10.3390/s19214668.
[18] R. Bajwa, E. Coleri, R. Rajagopal, P. Varaiya, and C. Flores, "Pavement performance assessment using a cost-effective wireless accelerometer system," *Computer-Aided Civil and Infrastructure Engineering*, vol. 35, no. 9, pp. 1009–1022, Sep. 2020, doi: https://doi.org/10.1111/mice.12544.
[19] Z. Ye, Y. Lu, and L. Wang, "Investigating the Pavement Vibration Response for Roadway Service Condition Evaluation," *Advances in Civil Engineering*, vol. 2018, p. 2714657, 2018, doi: 10.1155/2018/2714657.
[20] Y. Hou *et al.*, "The State-of-the-Art Review on Applications of Intrusive Sensing, Image Processing Techniques, and Machine Learning Methods in Pavement Monitoring and Analysis," *Engineering*, vol. 7, no. 6, pp. 845–856, 2021, doi: https://doi.org/10.1016/j.eng.2020.07.030.
[21] C. Zhang, S. Shen, H. Huang, and L. Wang, "Estimation of the Vehicle Speed Using Cross-Correlation Algorithms and MEMS Wireless Sensors," *Sensors*, vol. 21, no. 5, 2021, doi: 10.3390/s21051721.
[22] R. Rajagopal, R. Bajwa, E. Coleri, C. Flores, and P. Varaiya, *Sensor Network for Pavement Performance Monitoring*. 2013. doi: 10.1061/9780784413029.013.
[23] Z. Ye, H. Xiong, and L. Wang, "Collecting comprehensive traffic information using pavement vibration monitoring data," *Computer-Aided Civil and Infrastructure Engineering*, vol. 35, no. 2, pp. 134–149, Feb. 2020, doi: https://doi.org/10.1111/mice.12448.
[24] Z. Ye, Y. Lu, and L. Wang, "Investigating the Pavement Vibration Response for Roadway Service Condition Evaluation," *Advances in Civil Engineering*, vol. 2018, p. 2714657, 2018, doi: 10.1155/2018/2714657.
[25] S. Shen, L. Wang, C. Zhang, and D. Ildefonzo, "Use of SmartRock Sensors to Monitor Pavement Condition for Supporting Maintenance Decision Making," University Park, PA, Apr. 2022.
[26] M. Hallenbeck and H. Weinblatt, "Equipment for Collecting Traffic Load Data," Washington, DC, 2004.
[27] T. M. Kwon, "Implementation and Evaluation of a Low-Cost Weigh-In-Motion System," St. Paul, MN, 2016.

APPENDIX A

Additional Figures

TRIAL 1: NORMALIZED DATA

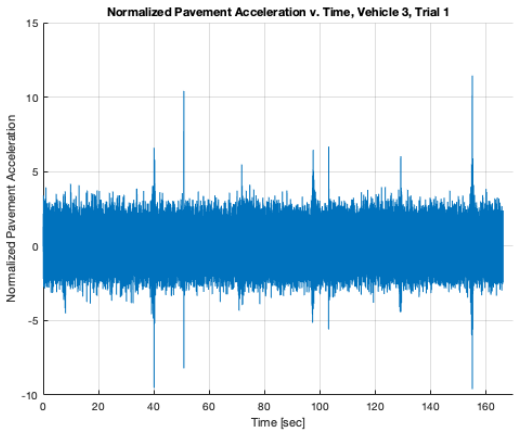

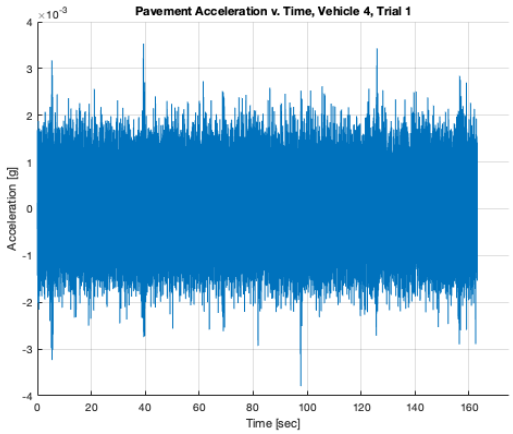

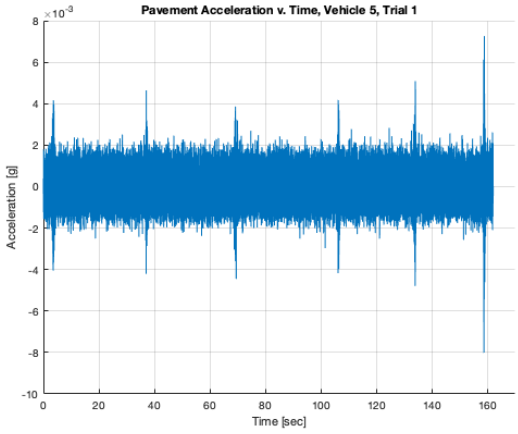

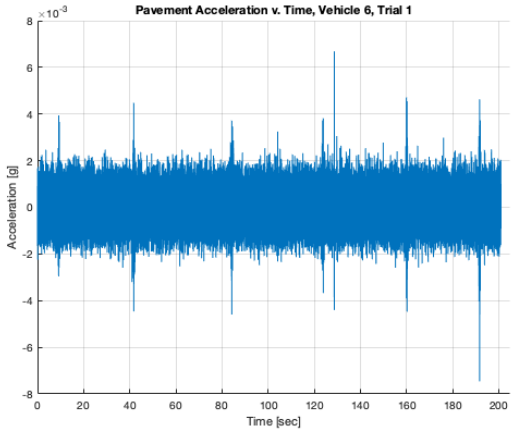

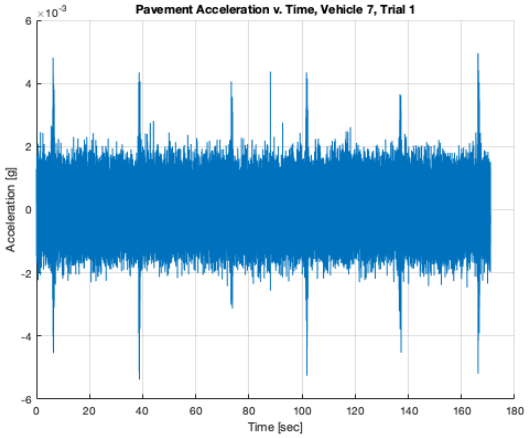

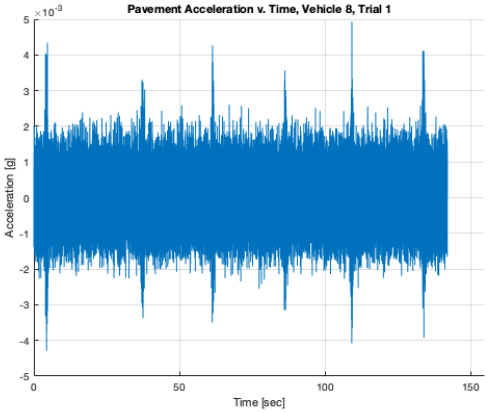

TRIAL 2: NORMALIZED DATA

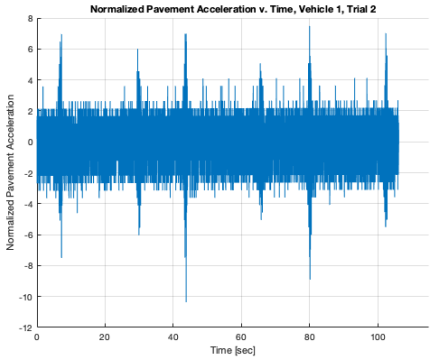

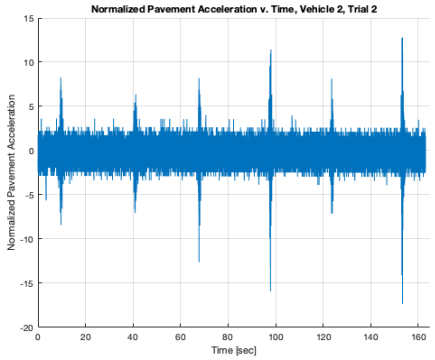

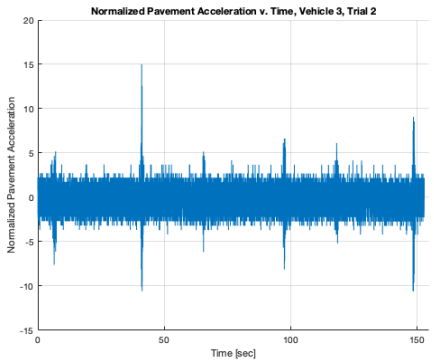

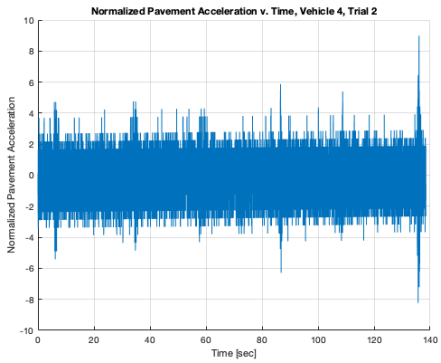

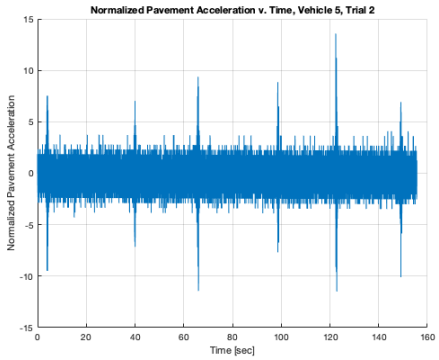

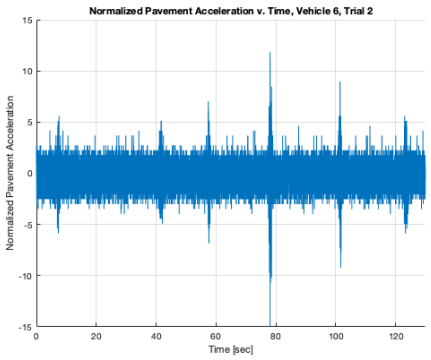

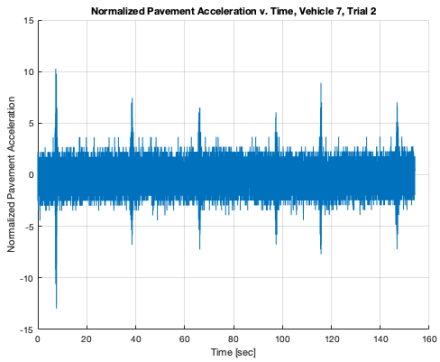

TRIAL 1: SPECTROGRAMS

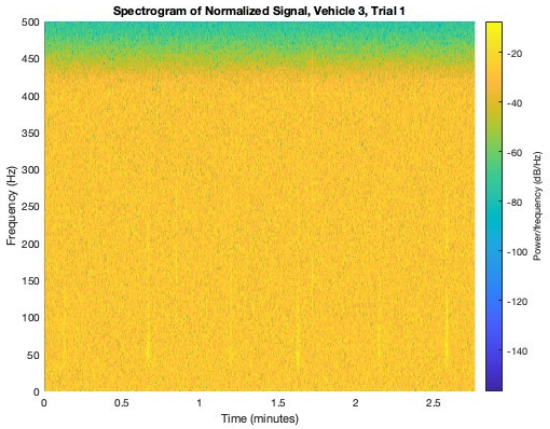

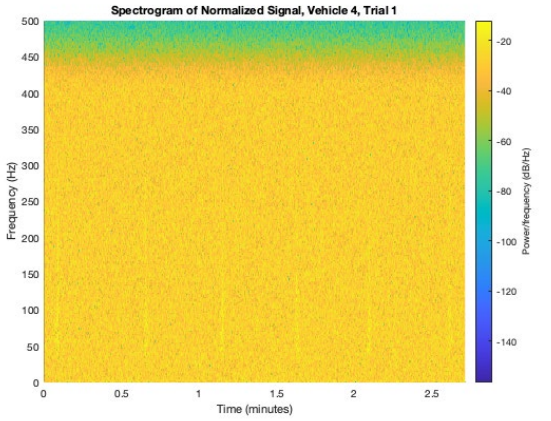

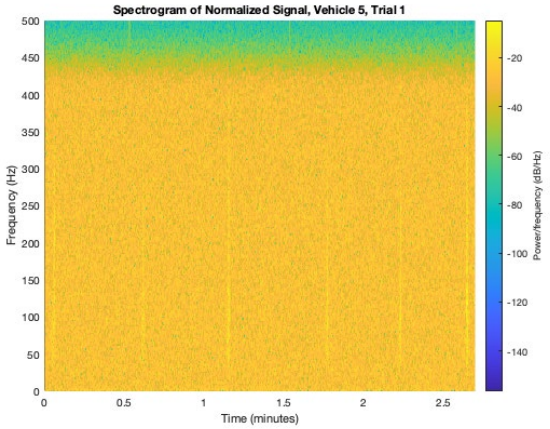

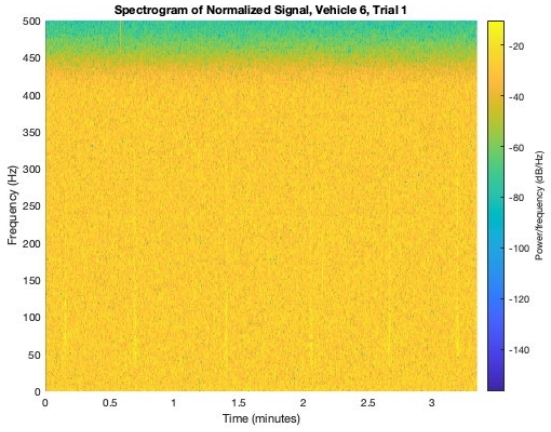

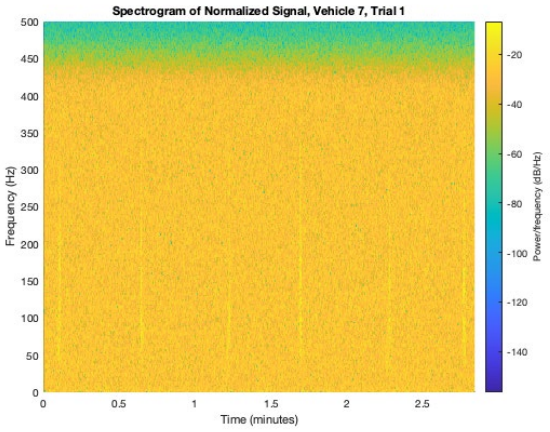

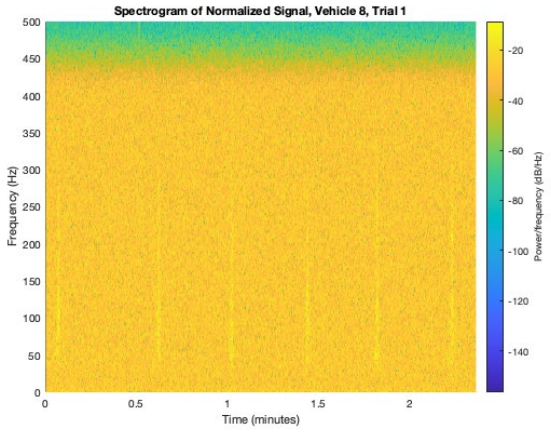

TRIAL 2: SPECTROGRAMS

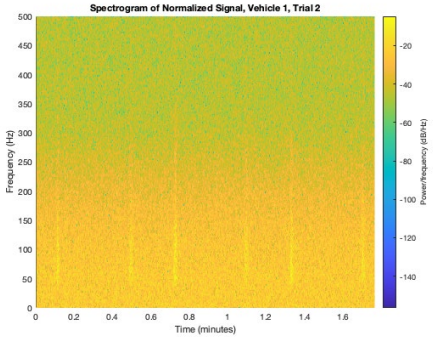

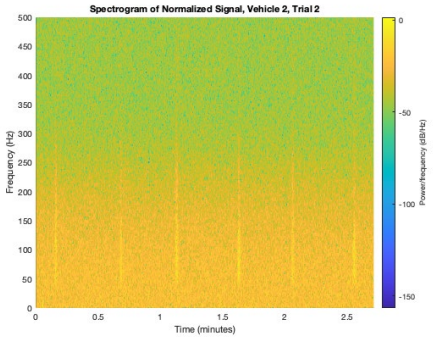

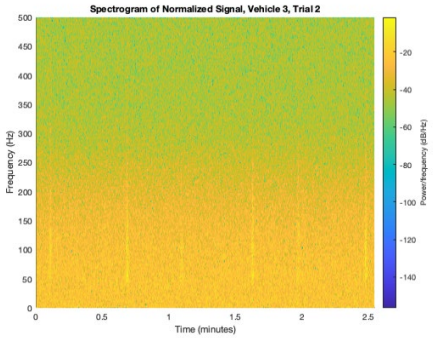

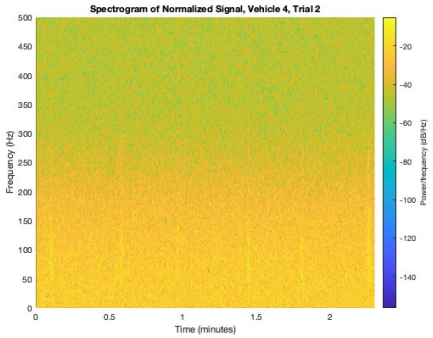

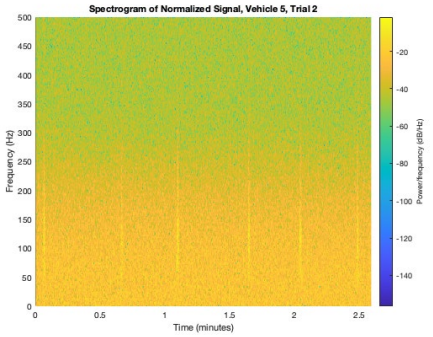

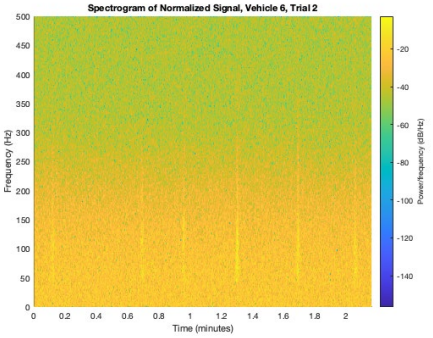

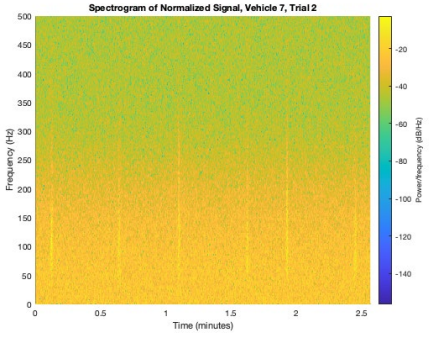

TRIAL 1: ROI PSD

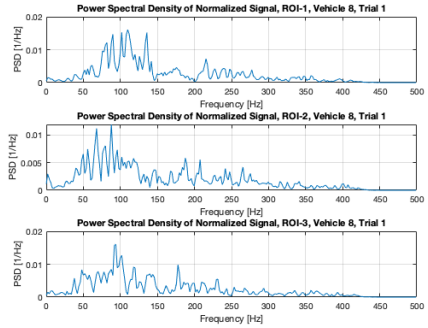

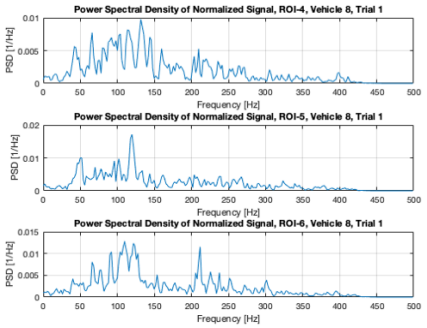

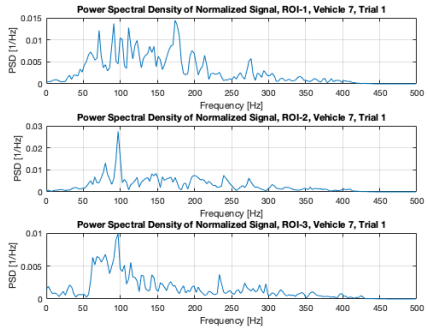

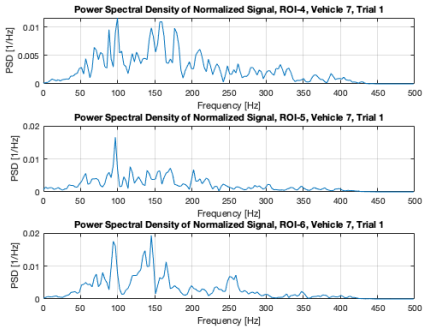

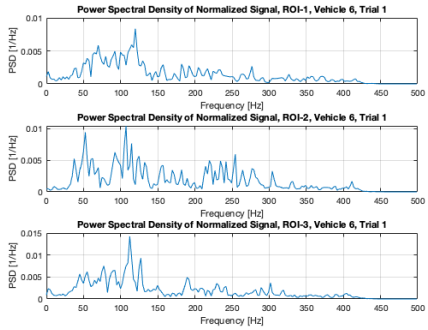

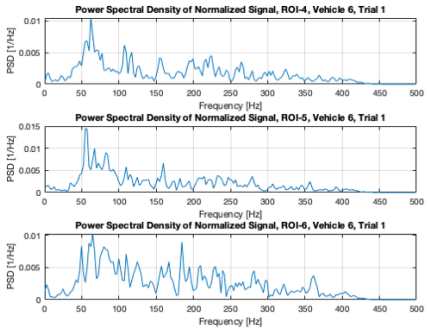

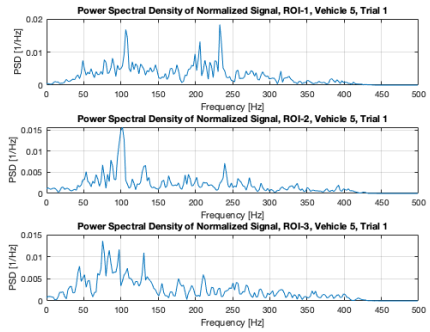

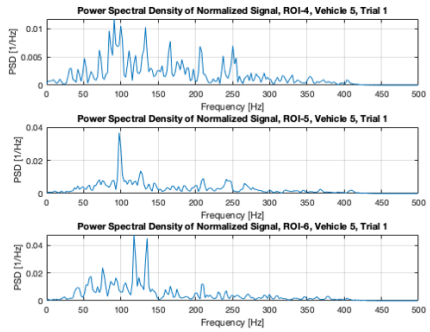

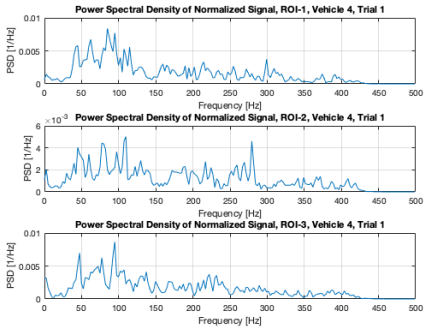
Power Spectral Density of Normalized Signal, ROI-1, Vehicle 4, Trial 1
PSD [1/Hz]
Frequency [Hz]

Power Spectral Density of Normalized Signal, ROI-2, Vehicle 4, Trial 1
PSD [1/Hz]
Frequency [Hz]

Power Spectral Density of Normalized Signal, ROI-3, Vehicle 4, Trial 1
PSD [1/Hz]
Frequency [Hz]

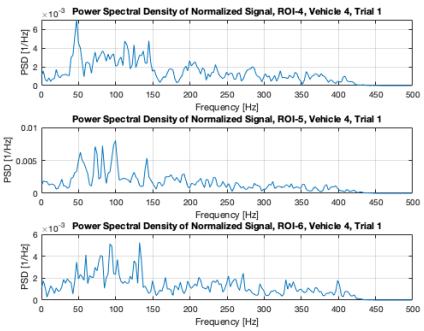
Power Spectral Density of Normalized Signal, ROI-4, Vehicle 4, Trial 1
PSD [1/Hz]
Frequency [Hz]

Power Spectral Density of Normalized Signal, ROI-5, Vehicle 4, Trial 1
PSD [1/Hz]
Frequency [Hz]

Power Spectral Density of Normalized Signal, ROI-6, Vehicle 4, Trial 1
PSD [1/Hz]
Frequency [Hz]

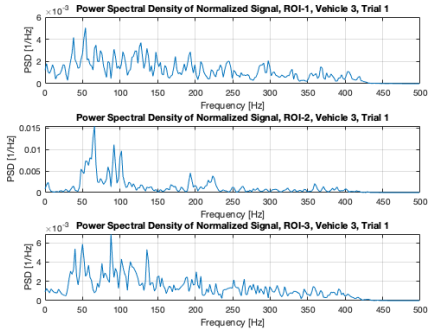
Power Spectral Density of Normalized Signal, ROI-1, Vehicle 3, Trial 1
PSD [1/Hz]
Frequency [Hz]

Power Spectral Density of Normalized Signal, ROI-2, Vehicle 3, Trial 1
PSD [1/Hz]
Frequency [Hz]

Power Spectral Density of Normalized Signal, ROI-3, Vehicle 3, Trial 1
PSD [1/Hz]
Frequency [Hz]

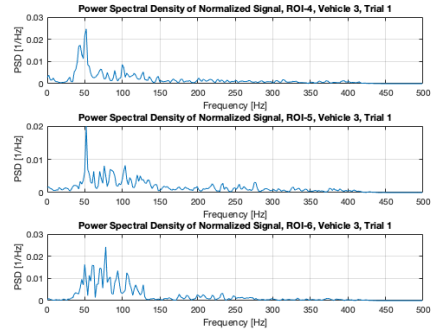
Power Spectral Density of Normalized Signal, ROI-4, Vehicle 3, Trial 1
PSD [1/Hz]
Frequency [Hz]

Power Spectral Density of Normalized Signal, ROI-5, Vehicle 3, Trial 1
PSD [1/Hz]
Frequency [Hz]

Power Spectral Density of Normalized Signal, ROI-6, Vehicle 3, Trial 1
PSD [1/Hz]
Frequency [Hz]

TRIAL 2: ROI PSD

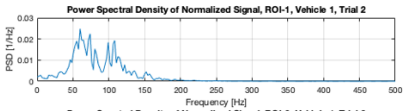

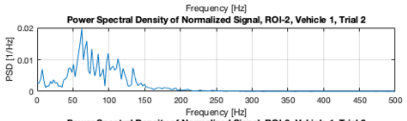

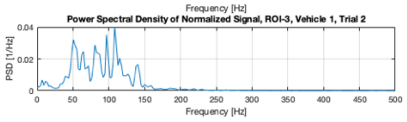

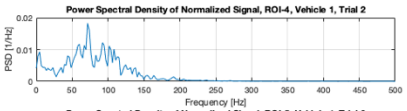

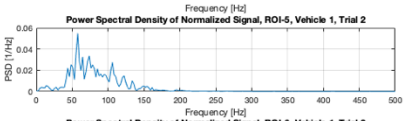

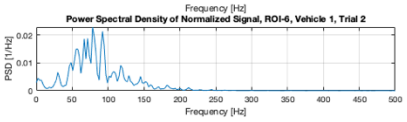

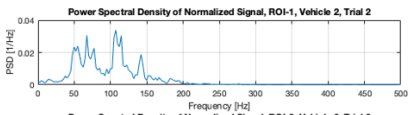

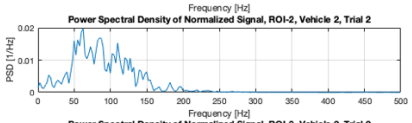

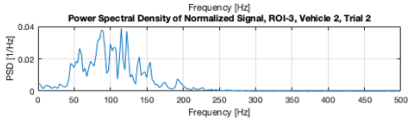

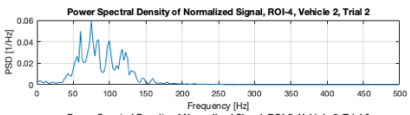

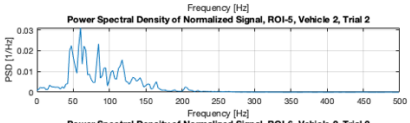

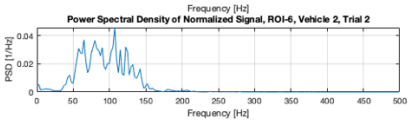

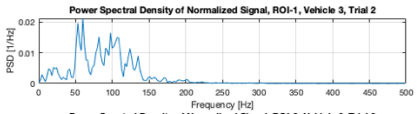

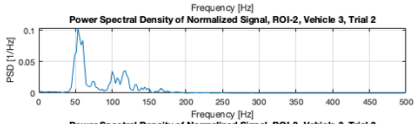

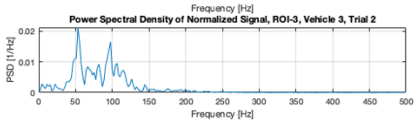

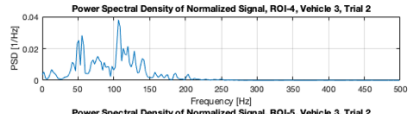

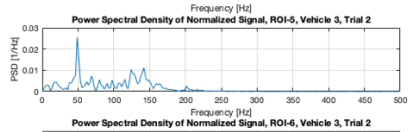

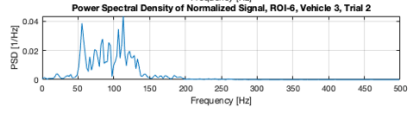

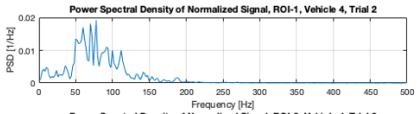

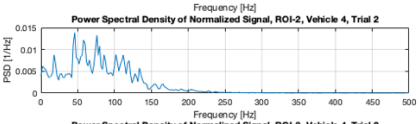

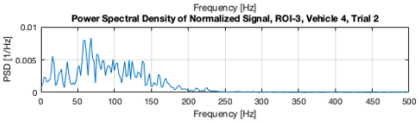

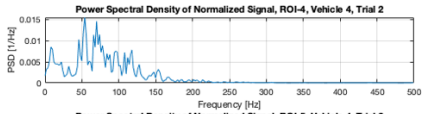

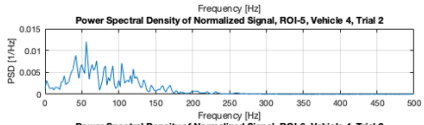

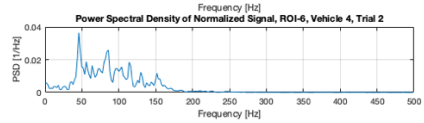

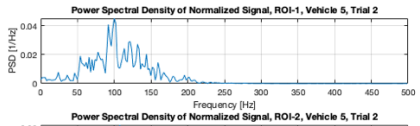
Power Spectral Density of Normalized Signal, ROI-1, Vehicle 5, Trial 2
PSD [1/Hz]
Frequency [Hz]

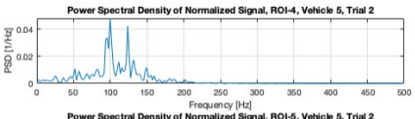
Power Spectral Density of Normalized Signal, ROI-4, Vehicle 5, Trial 2
PSD [1/Hz]
Frequency [Hz]

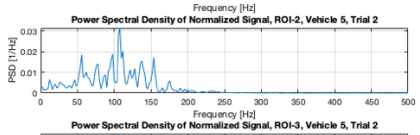
Power Spectral Density of Normalized Signal, ROI-2, Vehicle 5, Trial 2
PSD [1/Hz]
Frequency [Hz]

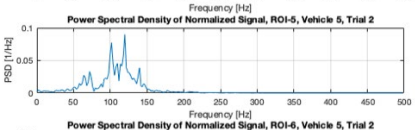
Power Spectral Density of Normalized Signal, ROI-5, Vehicle 5, Trial 2
PSD [1/Hz]
Frequency [Hz]

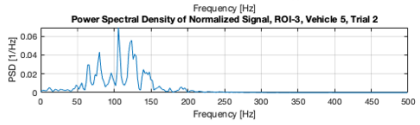
Power Spectral Density of Normalized Signal, ROI-3, Vehicle 5, Trial 2
PSD [1/Hz]
Frequency [Hz]

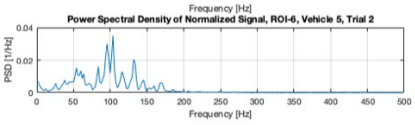
Power Spectral Density of Normalized Signal, ROI-6, Vehicle 5, Trial 2
PSD [1/Hz]
Frequency [Hz]

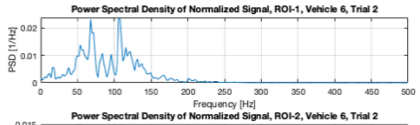
Power Spectral Density of Normalized Signal, ROI-1, Vehicle 6, Trial 2
PSD [1/Hz]
Frequency [Hz]

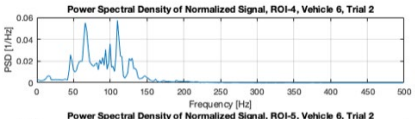
Power Spectral Density of Normalized Signal, ROI-4, Vehicle 6, Trial 2
PSD [1/Hz]
Frequency [Hz]

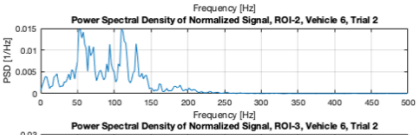
Power Spectral Density of Normalized Signal, ROI-2, Vehicle 6, Trial 2
PSD [1/Hz]
Frequency [Hz]

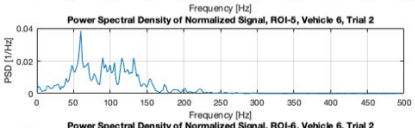
Power Spectral Density of Normalized Signal, ROI-5, Vehicle 6, Trial 2
PSD [1/Hz]
Frequency [Hz]

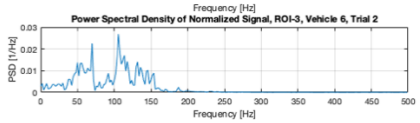
Power Spectral Density of Normalized Signal, ROI-3, Vehicle 6, Trial 2
PSD [1/Hz]
Frequency [Hz]

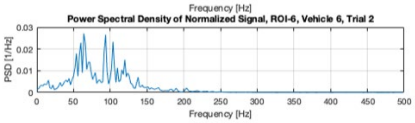
Power Spectral Density of Normalized Signal, ROI-6, Vehicle 6, Trial 2
PSD [1/Hz]
Frequency [Hz]

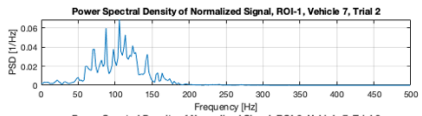
Power Spectral Density of Normalized Signal, ROI-1, Vehicle 7, Trial 2
PSD [1/Hz]
Frequency [Hz]

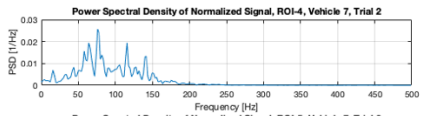
Power Spectral Density of Normalized Signal, ROI-4, Vehicle 7, Trial 2
PSD [1/Hz]
Frequency [Hz]

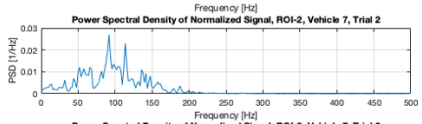
Power Spectral Density of Normalized Signal, ROI-2, Vehicle 7, Trial 2
PSD [1/Hz]
Frequency [Hz]

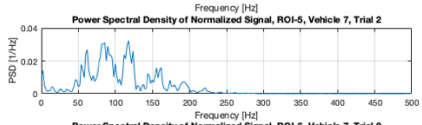
Power Spectral Density of Normalized Signal, ROI-5, Vehicle 7, Trial 2
PSD [1/Hz]
Frequency [Hz]

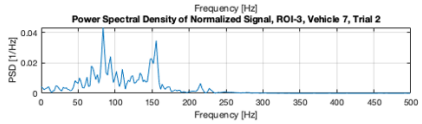
Power Spectral Density of Normalized Signal, ROI-3, Vehicle 7, Trial 2
PSD [1/Hz]
Frequency [Hz]

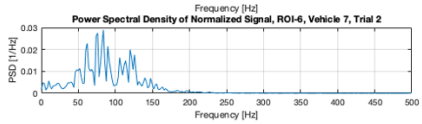
Power Spectral Density of Normalized Signal, ROI-6, Vehicle 7, Trial 2
PSD [1/Hz]
Frequency [Hz]